was performed using a PrimeScript High Fidelity RT-PCR kit (Takara Bio, Shiga, Japan); subsequent PCR reactions were performed using an RNA-LAPCR kit (Takara Bio) according to the manufacturer's instructions. β-Actin served as the internal control. The number of PCR cycles was set at 35 for Ad-KGF and at 25 for β-actin. The forward and reverse primer sequences for Ad-KGF and β-actin are listed in Table E1. Densitometry scanning was performed using NIH Image software (National Institute of Health, Rockville, MD).

Real-time PCR

Total RNA (to 100 ng) was transcribed using Superscript III reverse transcriptase (Invitrogen) and oligo-(dT). PCR amplification was performed on a Thermal Cycler Dice (Takara Bio) using SYBR Green I as a double-strand DNA-specific binding dye and continuous fluorescence monitoring according to the manufacturer's instructions. The forward and reverse primer sequences for each mRNA are listed in Table E2. β-Actin was used as the assay standard. The levels of expression of each mRNA and their estimated crossing points were determined relative to the standard preparation using the Thermal Cycler Dice computer software (Takara Bio). Expression data were normalized based on the expression levels of β-actin mRNA.

Western blotting for transforming growth factor (TGF)-β1 and SP-D

One lobe of the right lung was homogenized with an elution buffer containing 20 mM HEPES, pH 7.6, 20 mM NaCl, 0.5 mM EDTA, and 10% glycerol on ice. Standardized quantities of proteins were loaded onto SDS-PAGE gel and transferred electrophoretically onto nitrocellulose membranes. After the membranes were blocked with 0.5% skim milk in phosphate-buffered saline/0.1% Tween 20 (PBS-T), they were incubated with diluted primary antibody in PBS-T containing 0.5% skim milk for 1 h. The dilutions of primary antibodies were 1:2000 for TGF-β1, 1:2000 for SP-D, and 1:10000 for β-actin. Primary antibodies of TGF-β1 and SP-D were obtained from Santa Cruz Technology. The membranes were washed three times in PBS-T for 15 min and incubated for 30 min with peroxidase-conjugated IgG. After membranes were washed three times in PBS-T for 15 min, specific signals were visualized using an ECL system (GE Healthcare Life Science, Amersham, UK) and blots were exposed on X-ray films.

Statistics

Data are reported as means and SEM for each group. Comparisons of multiple groups were made with a Tukey-Kramer *post hoc* test after analysis of variance (ANOVA). Survival rates are shown on the basis of Kaplan-Meier product limit curves, and the groups were compared by log rank test. A $p < 0.05$ was considered significant.

References

E1. Kanegae Y, Makimura M, Saito I. A simple and efficient method for purification of infectious recombinant adenovirus. Jpn J Med Sci Biol 1994;47:157-166.

E2. Chaudhary NI, Schnapp A, Park JE: Pharmacologic differentiation of inflammation and fibrosis in the rat bleomycin model. Am J Respir Crit Care Med 2006;173:769-776.

E3. Hirai T, Hosokawa M, Kawakami K, Takubo Y, Sakai N, Oku Y, Chin K, Ohi M, Higuchi K, Kuno K, Mishima M. Age-related changes in the static and dynamic mechanical properties of mouse lungs. Respir Physiol. 1995;102:195-203.

Tables

Table E1. Primer sequences for RT-PCR

Gene	Forward primer	Reverse primer
β-actin	5'-GGCCAACCGTGAAAAGATGAC	5'-ATTGCCGATAGTGATGACCTG
Ad-mKGF	5'-GACCCAGGAGATGAAGAA	5'-CTAGACTAGTTTAATTAA

Ad-mKGF, adenovirus vector for murine keratinocyte growth factor

Table E2. Primer sequences for SYBR-green-based real-time PCR

Gene	Forward primer	Reverse primer
β-actin	5'-CATCCGTAAAGACCTCTATGCCAAC	5'-ATGGAGCCACCGATCCACA
KGF	5'-TGGTACCTGAGGATTGACAAACGA	5'-CCTTTGATTGCCACAATTCCAAC
SP-A	5'-CTCGGAGGCAGACATCCACA	5'-TGATGCCAGCAACAACAGTCAA
SP-B	5'-GAGTGTGCACAAGGCCCTCA	5'-CCTCACACTCTTGGCACAGGTC
SP-C	5'-CATCATGAAGATGGCTCCAGAGA	5'-ACACAGGGTGCTCACAGCAAG
SP-D	5'- CCTCAAGGCAAACCAGGTCCTA	5'-TGCATGCCAGGAGCACCTAC
Col 1a	5'-CAGGGTATTGCTGGACAACGTG	5'-GGACCTTGTTTGCCAGGTTCA
Col 3a	5'-CCACGTAAGCACTGGTGGACA	5'-GCCAGCTGCACATCAACGA

KGF, keratinocyte growth factor; SP, surfactant protein; Col, collagen

Figure Legends

Figure E1. Representative microphotographs of bleomycin-induced subpleural inflammation in the saline (A), 1w1 (B), and KGF (C) groups 2 weeks after bleomycin administration and 1 week after saline, Ad-1w1, or Ad-KGF instillation, respectively. Intra-alveolar inflammatory cell infiltration was not considerably different among the three groups (hematoxylin and eosin stain). Black bars, 100 mm.

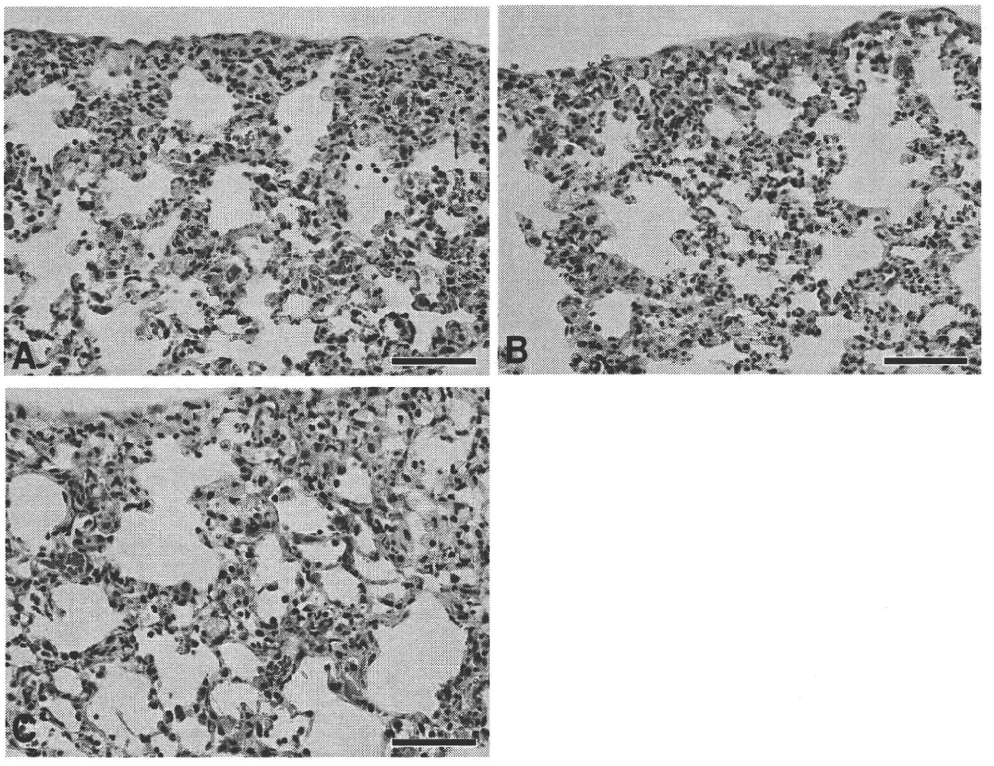

Fig. E1

Persistent expression of the full genome of hepatitis C virus in B cells induces spontaneous development of B-cell lymphomas in vivo

*Yuri Kasama,[1] *Satoshi Sekiguchi,[2] Makoto Saito,[1] Kousuke Tanaka,[1] Masaaki Satoh,[1] Kazuhiko Kuwahara,[3] Nobuo Sakaguchi,[3] Motohiro Takeya,[4] Yoichi Hiasa,[5] Michinori Kohara,[2] and Kyoko Tsukiyama-Kohara[1]

[1]Department of Experimental Phylaxiology, Faculty of Life Sciences, Kumamoto University, Kumamoto, Japan; [2]Department of Microbiology and Cell Biology, Tokyo Metropolitan Institute of Medical Science, Tokyo, Japan; [3]Department of Immunology, Faculty of Life Sciences, Kumamoto University, Kumamoto, Japan; [4]Department of Cell Pathology, Faculty of Life Sciences, Kumamoto University, Kumamoto, Japan; and [5]Department of Gastroenterology and Metabology, Ehime University Graduate School of Medicine, To-on, Ehime, Japan

Extrahepatic manifestations of hepatitis C virus (HCV) infection occur in 40%-70% of HCV-infected patients. B-cell non-Hodgkin lymphoma is a typical extrahepatic manifestation frequently associated with HCV infection. The mechanism by which HCV infection of B cells leads to lymphoma remains unclear. Here we established HCV transgenic mice that express the full HCV genome in B cells (RzCD19Cre mice) and observed a 25.0% incidence of diffuse large B-cell non-Hodgkin lymphomas (22.2% in males and 29.6% in females) within 600 days after birth. Expression levels of aspartate aminotransferase and alanine aminotransferase, as well as 32 different cytokines, chemokines and growth factors, were examined. The incidence of B-cell lymphoma was significantly correlated with only the level of soluble interleukin-2 receptor α subunit (sIL-2Rα) in RzCD19Cre mouse serum. All RzCD19Cre mice with substantially elevated serum sIL-2Rα levels (> 1000 pg/mL) developed B-cell lymphomas. Moreover, compared with tissues from control animals, the B-cell lymphoma tissues of RzCD19Cre mice expressed significantly higher levels of IL-2Rα. We show that the expression of HCV in B cells promotes non-Hodgkin–type diffuse B-cell lymphoma, and therefore, the RzCD19Cre mouse is a powerful model to study the mechanisms related to the development of HCV-associated B-cell lymphoma. (*Blood*. 2010;116(23):4926-4933)

Introduction

More than 175 million people worldwide are infected with hepatitis C virus (HCV), a positive-strand RNA virus that infects both hepatocytes and peripheral blood mononuclear cells.[1] Chronic HCV infection may lead to hepatitis, liver cirrhosis, hepatocellular carcinomas[2,3] and lymphoproliferative diseases such as B-cell non-Hodgkin lymphoma and mixed-cryoglobulinemia.[1,4-6] B-cell non-Hodgkin lymphoma is a typical extrahepatic manifestation frequently associated with HCV infection[7] with geographic and ethnic variability.[8,9] Based on a meta-analysis, the prevalence of HCV infection in patients with B-cell non-Hodgkin lymphoma is approximately 15%.[8] The HCV envelope protein E2 binds human CD81,[10] a tetraspanin expressed on various cell types including lymphocytes, and activates B-cell proliferation[11]; however, the precise mechanism of disease onset remains unclear. We previously developed a transgenic mouse model that conditionally expresses HCV cDNA (nucleotides 294-3435), including the viral genes that encode the core, E1, E2, and NS2 proteins, using the Cre/*lox*P system (in core~NS2 [CN2] mice).[12,13] The conditional transgene activation of the HCV cDNA (core, E1, E2, and NS2) protects mice from Fas-mediated lethal acute liver failure by inhibiting cytochrome c release from mitochondria.[13] In HCV-infected mice, persistent HCV protein expression is established by targeted disruption of *irf-1*, and high incidences of lymphoproliferative disorders are found in CN2 *irf-1*$^{-/-}$ mice.[14] Infection and replication of HCV also occur in B cells,[15,16] although the direct effects, particularly in vivo, of HCV infection on B cells have not been clarified.

To define the direct effect of HCV infection on B cells in vivo, we crossed transgenic mice with an integrated full-length HCV genome (Rz) under the conditional Cre/*lox*P expression system with mice expressing the Cre enzyme under transcriptional control of the B lineage–restricted gene *CD19*,[17] we addressed the effects of HCV transgene expression in this study.

Methods

Animal experiments

Wild-type (WT), Rz, CD19Cre, RzCD19Cre mice (129/sv, BALB/c, and C57BL/6J mixed background), and MxCre/CN2-29 mice (C57BL/6J background) were maintained in conventional animal housing under specific pathogen-free conditions. All animal experiments were performed according to the guidelines of the Tokyo Metropolitan Institute of Medical Science or the Kumamoto University Subcommittee for Laboratory Animal Care. The protocol was approved by the Institutional Review Boards of both facilities.

Measurements of HCV protein and RNA

Mice were anesthetized and bled, and tissues (spleen, lymph nodes, liver, and tumors) were homogenized in lysis buffer (1% sodium dodecyl sulfate; 0.5% (wt/vol) nonyl phenoxypolyethoxylethanol; 0.15M NaCl; 10 mM

Submitted May 2, 2010; accepted August 13, 2010. Prepublished online as *Blood* First Edition paper, August 23, 2010; DOI 10.1182/blood-2010-05-283358.

*Y.K. and S.S. contributed equally to this work.

The online version of this article contains a data supplement.

The publication costs of this article were defrayed in part by page charge payment. Therefore, and solely to indicate this fact, this article is hereby marked "advertisement" in accordance with 18 USC section 1734.

tris(hydroxymethyl)aminomethane, pH 7.4) using a Dounce homogenizer. The concentration of HCV core protein in tissue lysates was measured using an HCV antigen enzyme-linked immunosorbent assay (ELISA; Ortho).[18] HCV mRNA was isolated by a guanidine thiocyanate protocol using ISOGEN (Nippon Gene) and was detected by reverse transcription polymerase chain reaction (RT-PCR) amplification using primers specific for the 5′ untranslated region of the *HCR6* sequence.[19,20] Reverse transcription was performed using Superscript III reverse transcriptase (Invitrogen) with random primers. PCR primers NCR-F (5′-TTCACGCAGAAAGCGTCTAGCCAT-3′) and NCR-R (5′-TCGTCCTGGCAATTCCGGTGTACT-3′) were used for the first round of HCV cDNA amplification, and the resulting product was used as a template for a second round of amplification using primers NCR-F INNER (5′-TTCCGCAGACCACTATGGCT-3′) and NCR-R INNER (5′-TTCCGCAGACCACTATGGCT-3′).

Collection of serum for chemokine ELISA

Blood samples were collected from the supraorbital veins or by heart puncture of killed mice. Blood samples were centrifuged at 10 000*g* for 15 minutes at 4°C to isolate the serum.[21] Serum concentrations of interleukin (IL)–1α, IL-1β, IL-2, IL-3, IL-4, IL-5, IL-6, IL-9, IL-10, IL-12(p40), IL-12(p70), IL-13, IL-17, Eotaxin, granulocyte colony-stimulating factor (CSF), granulocyte–macrophage–CSF, interferon (IFN)–γ, keratinocyte-derived chemokine (KC), monocyte chemotactic protein-1, macrophage inflammatory protein (MIP)–1α, MIP-1β, Regulated upon Activation, Normal T-cell Expressed, and Secreted, tumor necrosis factor-α, IL-15, fibroblast growth factor-basic, leukemia inhibitory factor, macrophage-CSF, human monokine induced by gamma interferon, MIP-2, platelet-derived growth factorβ, and vascular endothelial growth factor were measured using the Bio-Plex Pro assay (Bio-Rad). Serum soluble IL-2 receptor α (sIL-2Rα) concentrations were determined by ELISA (DuoSet ELISA Development System; R&D Systems). Serum aspartate aminotransferase (AST) and alanine aminotransferase (ALT) activities were determined using a commercially available kit (Transaminase CII test; Wako Pure Chemical Industries).

Histology and immunohistochemical staining

Mouse tissues were fixed with 4% formaldehyde (Mildform 10 N; Wako Pure Chemical Industries), dehydrated with an ethanol series, embedded in paraffin, sectioned (10-μm thick) and stained with hematoxylin and eosin. For tissue immunostaining, paraffin was removed from the sections using xylene following the standard method,[14] and sections were incubated with anti-CD3 or anti-CD45R (Santa Cruz Biotechnology) in phosphate-buffered saline without Ca^{2+} and Mg^{2+} (pH 7.4) but with 5% skim milk. Next, the sections were incubated with biotinylated anti-rat immunoglobulin (Ig)G (1:500), followed by incubation with horseradish peroxidase-conjugated avidin-biotin complex (Dako Corp), and the color reaction was developed using 3,3′-diaminobenzidine. Sections were observed under an optical microscope (Carl Zeiss).

Detection of immunoglobulin gene rearrangements by PCR

Genomic DNA was isolated from tumor tissues, and PCR was performed as described.[22] In brief, PCR reaction conditions were 98°C for 3 minutes; 30 cycles at 98°C for 30 seconds, 60°C for 30 seconds, 72°C for 1.5 minutes, and 72°C for 10 minutes. Mouse Vk genes were amplified using previously described primers.[23] Amplification of mouse Vj genes was performed using Vκcon (5′-GGCTGCAGSTTCAGTGGCAGTGGRTCWGGRAC-3′; R, purine; W, A or T) and Jκ5 (5′-TGCCACGTCAACTGATAATGAGCCCTCTC-3′) as described.[24]

Results

Establishment of transgenic mice with B lineage–restricted HCV gene expression

We defined the direct effect of HCV infection on B cells in vivo by crossing transgenic mice that had an integrated full-length HCV genome (Rz) under the conditional Cre/*lox*P expression system (Figure 1A upper schematic)[12,19,25] with mice that expressed the Cre enzyme under transcriptional control of the B lineage–restricted gene *CD19*[17] (RzCD19Cre; Figure 1A lower schematic). Expression of the HCV transgene in RzCD19Cre mice was confirmed by ELISA (Figure 1B); a substantial level of HCV core protein was detected in the spleen (370.9 ± 10.2 pg/mg total protein), but levels were lower in the liver (0.32 ± 0.03 pg/mg) and plasma (not detectable). RT-PCR analysis of peripheral blood lymphocytes (PBLs) from RzCD19Cre mice indicated the presence of HCV transcripts (Figure 1C). The weights of RzCD19Cre, Rz (with the full HCV genome transgene alone), CD19Cre (with the Cre gene knock-in at the CD19 gene locus) and WT mice were measured weekly for more than 600 days post birth; there were no significant differences between these groups (data not shown; the total number of transgenic and WT mice was approximately 200). The survival rate in each group was also measured for > 600 days (Figure 1D); survival in the female RzCD19Cre group was lower than that of the other groups.

The spontaneous development of B-cell lymphomas in the RzCD19Cre mouse

At 600 days post birth, mice (n = 140) were killed by bleeding under anesthesia, and tissues (spleen, lymph node, liver, and tumors) were excised and examined by hematoxylin and eosin staining (Figure 2A; supplemental Figure 1, available on the *Blood* Web site; see the Supplemental Materials link at the top of the online article). The incidence of B-cell lymphoma in RzCD19Cre mice was 25.0% (22.2% in males and 29.6% in females) and was significantly higher than the incidence in the HCV-negative groups (Table 1). This incidence is significantly higher than those of the other cell-type tumors developed spontaneously in all mouse groups (supplemental Table 1). Because nodular proliferation of CD45R-positive atypical lymphocytes was observed, lymphomas were diagnosed as typical diffuse B-cell non-Hodgkin lymphomas (Figure 2Aiv,vi-vii; supplemental Figure 1B,E,H,M). Mitotic cells were also positive for CD45R (Figure 2Avi arrowheads). CD3-positive T-lymphocytes were small and had a scattered distribution. Intrahepatic lymphomas had the same immunophenotypic characteristics as B-cell lymphomas (supplemental Figure 1K arrowheads, inset; 1L–N, ID No. 24-4, RzCD19Cre mouse); lymphoma tissues were markedly different compared with the control lymph node (Figure 2Ai,iii,v; ID No. 47-4, CD19Cre mouse) and liver (supplemental Figure 1J; ID No. 24-2, Rz mouse; tissues were from a littermate of the mice used to generate the data in supplemental Figure 1D-I,K-N). All samples were reviewed by at least 2 expert pathologists and classified according to World Health Organization classification.[26] Lymphomas were mostly CD45R positive and located in the mesenteric lymph nodes (Figure 2A; supplemental Figure 1), and some were identified as intrahepatic lymphomas (incidence, 4.2%; supplemental Figure 1K-N). HCV gene expression was detected in all B-cell lymphomas of RzCD19Cre mice (Figure 2B).

To examine the Ig gene configuration in the B-cell lymphomas of the RzCD19Cre mice, genomic DNA was isolated and analyzed by PCR. Ig gene rearrangements were identified in each case (Figure 2C). Genomic DNA isolated from the tumors of a germinal center–associated nuclear protein (GANP) transgenic mouse (GANP Tg#3) yielded a predominant Jk5 PCR product (Figure 2C, Vκ-Jκ); a predominant JH1 product and a minor JH2 product (supplemental Figure 2, DH-JH) were also identified, as previously reported,[22] indicating that the lymphoma cells proliferated from the transformation of an oligo B-cell clone. The B-cell lymphomas of

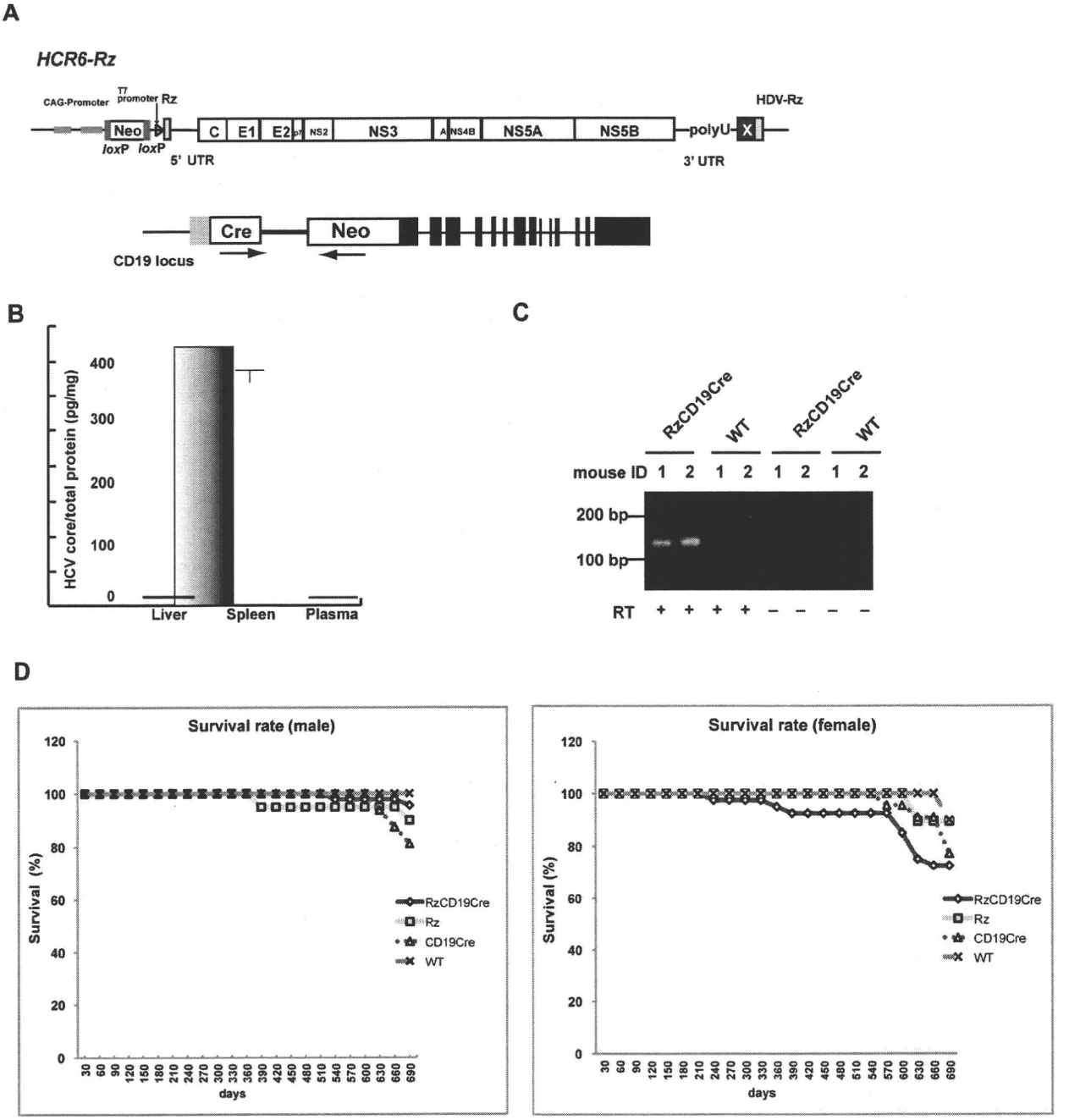

Figure 1. Establishment of RzCD19Cre mice. (A) Schematic diagram of the transgene structure comprising the complete HCV genome (*HCR6-Rz*). HCV genome expression was regulated by the Cre/*lox*P expression cassette (top diagram). The Cre transgene was located in the CD19 locus (bottom diagram). (B) Expression of HCV core protein in the liver, spleen, and plasma of RzCD19Cre mice was quantified by core ELISA. Data represent the mean ± SD (n = 3). (C) Detection of HCV RNA in PBLs by RT-PCR. Samples that included the RT reaction are indicated by +, and those that did not include the RT reaction are indicated by –. (D) Survival rates of male and female RzCD19Cre mice (males, n = 45; females, n = 40), Rz mice (males, n = 20; females, n = 19), CD19Cre mice (males, n = 16; females, n = 22), and WT mice (males, n = 5; females, n = 10).

8 RzCD19Cre mice (mouse ID Nos. 24-1, 54-1, 56-5, 69-5, 42-4, 43-4, 36-3 [data not shown] and 62-2 [data not shown]) yielded a Jκ-5 gene amplification product, and the lymphomas from 3 other mice had the alternative gene configurations Jκ-1 (mouse ID No. 31-4), Jκ-2 (mouse ID No. 24-4) and Jκ-3 (mouse ID No. 42-4; Figure 2C). PCR amplification products from the genes JH4 (mouse ID Nos. 24-1, 24-4, 54-1, 43-4, 56-5, 69-5, 62-2 [data not shown], 36-3 [data not shown]), JH1 (mouse ID Nos. 31-4, 42-4) and JH3 (mouse ID Nos. 31-4, 42-4, 56-5, 43-4, 36-3 [data not shown]) were also detected (supplemental Figure 2). The mutation frequencies in the Jκ-1, -3 and -5 genes were the same as the mutation frequency in the genomic V-region gene.[22] Few or no sequence differences in the variable region were identified among clones from which DNA was amplified. These results indicate the possibility that tumors judged as B-cell lymphomas based on pathology criteria were derived from the transformation of a single germinal center of B-cell origin.

To rule out the oncogenic effect caused by a transgenic integration into a specific genomic locus, we examined if HCV transgene inserted into another genomic site also causes B-cell lymphomas using another HCV transgenic mouse strain, MxCre/CN2-29 (supplemental Figure 3). Expression of the HCV CN2

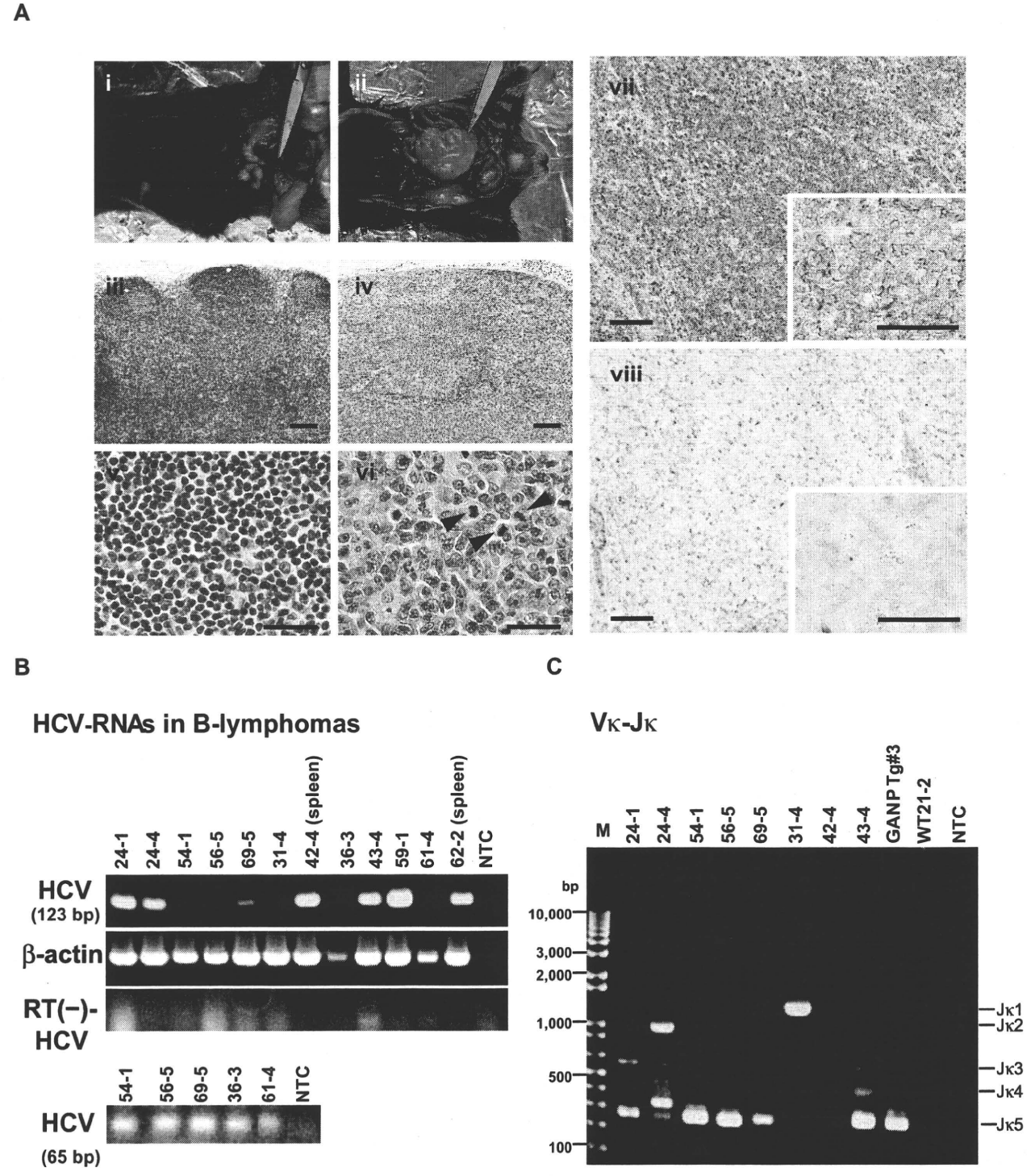

Figure 2. Histopathologic analysis of B-cell lymphomas in RzCD19Cre mouse tissues. (A) Histologic analysis of tissues from a normal mouse (i, iii, v; CD19Cre mouse, ID No. 47-4, male) and a B-cell lymphoma from a RzCD19Cre mouse (ii, iv, vi; ID No. 69-5, male). Paraformaldehyde-fixed and paraffin-embedded tumor tissues were stained with hematoxylin and eosin (iii-vi) or immunostained using anti-CD45R (vii; bottom right, inset) and anti-CD3 (viii; bottom right, inset). Also shown is a macroscopic view of the lymphoma from a mesenchymal lymph node (ii, indicated by forceps), which is not visible in the normal mouse (i). Mitotic cells are indicated with arrowheads (vi). Scale bars: 100 μm (iii-iv, vii-viii) and 20 μm (v-vi, insets in vii-viii). (B) Expression of HCV RNA in B-cell lymphomas from RzCD19Cre mice was examined by RT-PCR. The first round of PCR amplification yielded a 123-base pair fragment of HCV cDNA (upper panel), and a second round of PCR amplification yielded a 65-base pair fragment (lower panel). The β-actin mRNA was a control. As an additional control, the first and second rounds of amplification were performed using samples that had not been subjected to reverse transcription. NTC, no-template control. (C) Ig gene rearrangements in the tumors of RzCD19Cre mice. Genomic DNA isolated from B-cell lymphoma tissues of RzCD19Cre mice (ID Nos. 24-1, 24-4, 54-1, 56-5, 69-5, 31-4, 42-4, 43-4) and spleen tissues of a WT mouse (ID No. 21-2) was PCR amplified using primers specific for Vκ-Jκ genes. Amplification of controls was performed using genomic DNA isolated from a GANP transgenic mouse (GANP Tg#3) and in the absence of template DNA (no-template control, NTC). M, DNA ladder marker.

gene (nucleotides 294-3435)[12] was induced by the Mx promoter-driven cre recombinase with poly(I:C) induction[14] (supplemental Figure 3A). HCV core proteins were detected in both normal spleen (mouse ID Nos. 2, 3, 4) and intra-splenic B-cell lymphoma tissues

Table 1. Lymphoma incidence in HCV-expressing and control mice

HCV expression	Mouse genotype	No.	Incident B lymphoma, number (%)	Incident T lymphoma, number (%)
+	RzCD19Cre	72	18 (25.0)	3 (4.1)
−	Rz	34	1 (2.9)	1 (2.9)
−	CD19Cre	22	2 (9.1)	1 (4.5)
−	WT	12	1 (8.3)	1 (8.3)

(mouse ID Nos. 5, 6, 7) of MxCre/CN2-29 mice but not in spleens of the CN2-29 mouse (mouse ID No. 1, Figure 3B). After 12 months, the MxCre/CN2-29 mice developed B-cell lymphomas in the spleen at a high incidence (33.3%: 3/9), whereas the CN2-29 mice did not (0/13; supplemental Figure 3C), indicating that the development of B-cell lymphomas in HCV transgenic mice occurred similarly to RzCD19Cre mice. MxCre/CN2-29 mice also developed hepatocellular carcinomas (10%, 360 days, 17%, 480 days, 50%, 600 days after onset of HCV expression; Sekiguchi et al, submitted).

The results obtained in 2 HCV transgenic mouse strains indicate that the expression of the HCV gene or the proteins indeed induces the spontaneous development of B-cell lymphomas irrespective of the integrated site in the mouse genome.

The levels of cytokines and chemokines in B-cell lymphomas and other tumors and in tumor-free control mice

Abnormal induction of cytokine production occurs in HCV-associated non-Hodgkin lymphomas[27,28] and in patients with

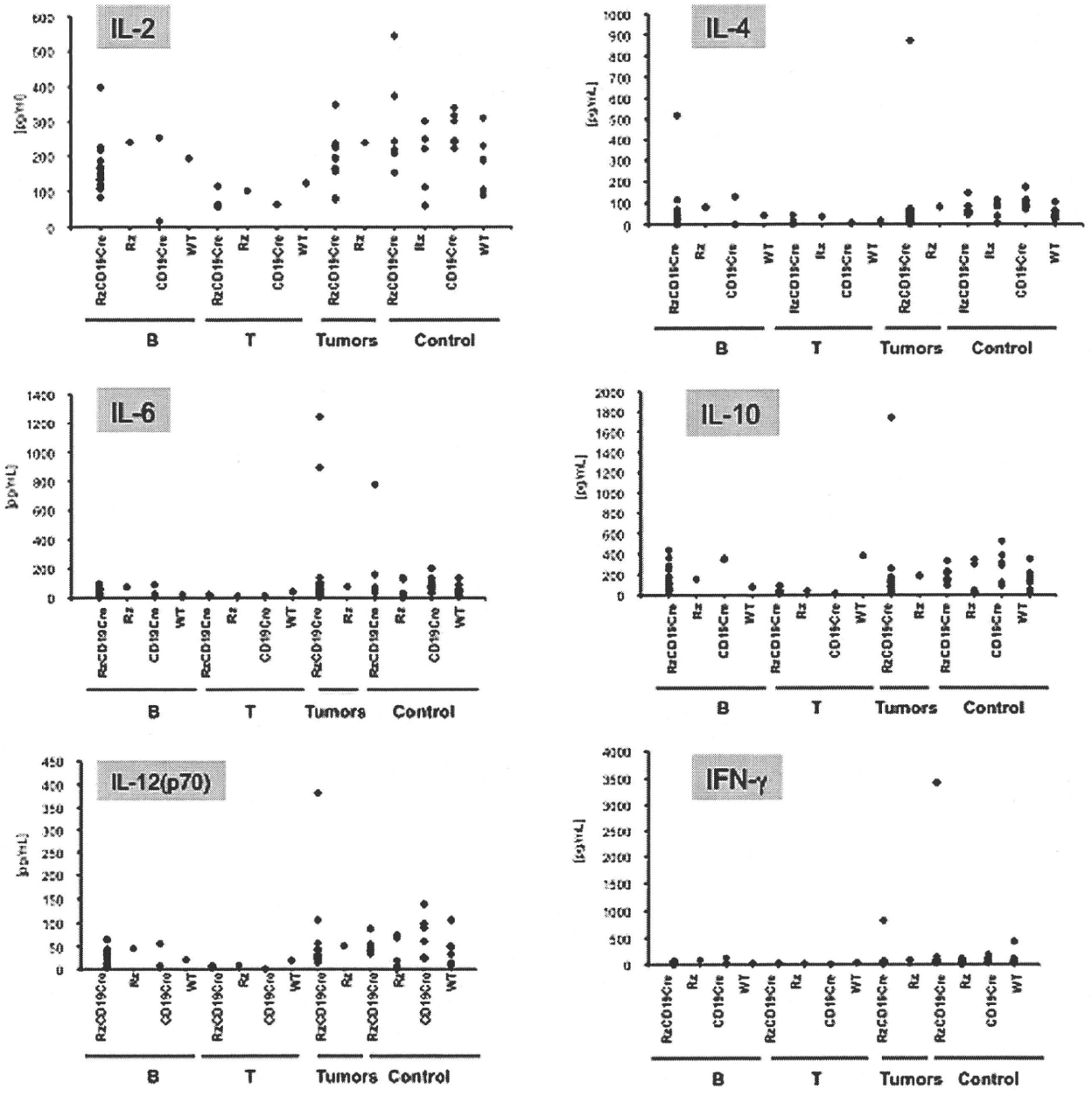

Figure 3. Analysis of serum cytokine levels using a multisuspension array system. The serum concentration levels of IL-2, IL-4, IL-6, IL-10, IL-12(p70), and IFN-γ were measured in RzCD19Cre mice with B-cell lymphomas (B), T-cell lymphomas (T), and other tumors (mammary tumor, sarcoma, and hepatocellular carcinoma) and in tumor-free RzCD19Cre, Rz, CD19Cr,e and WT mice.

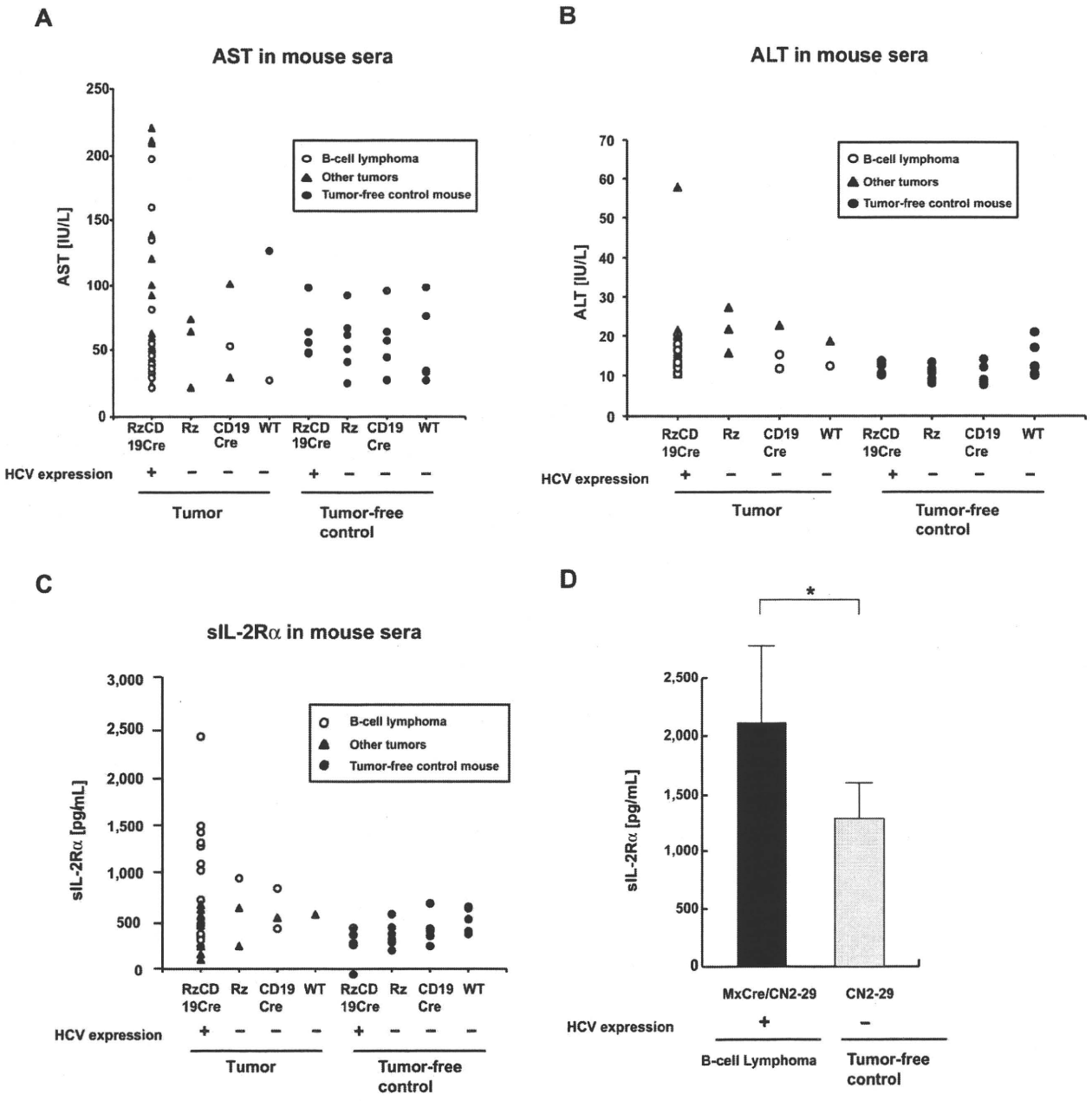

Figure 4. Serum titers of AST, ALT and soluble IL-2Rα in transgenic and control mice lacking or harboring B-cell lymphomas. (A-B) The AST (A) and ALT (B) assays were performed on serum samples from tumor-free control mice and the RzCD19Cre, Rz, CD19Cre and WT mice with or without B-cell lymphomas or other tumors. (C) ELISA analysis was performed to determine the sIL-2Rα concentration in serum samples from tumor-free control mice and the RzCD19Cre, Rz, CD19Cre, and WT mice with or without B-cell lymphomas or other tumors. (D) Concentration of soluble IL-2Rα in sera from transgenic (MxCre/CN2-29 or CN2-29) mice with or without B-cell lymphomas (*$P < .05$).

chronic hepatitis.[29,30] Therefore, we examined tumor cytokine and chemokine levels using a multisuspension array system. The levels of IL-2, IL-4, IL-6, IL-10, IL-12(p70), and IFN-γ (Figure 3), which may have a link with lymphoproliferation[14] or lymphoma[28,31] induced by HCV, and IL-1α, IL-1β, IL-3, IL-5, IL-9, IL-12(p40), IL-13, IL-17, Eotaxin, granulocyte-CSF, granulocyte–macrophage–CSF, KC, monocyte chemotactic protein-1, MIP-1α, MIP-1β, Regulated upon Activation, Normal T-cell Expressed, and Secreted, tumor necrosis factor-α, IL-15, fibroblast growth factor-basic, leukemia inhibitory factor, macrophage-CSF, human monokine induced by gamma interferon, MIP-2, platelet-derived growth factorβ and vascular endothelial growth factor (supplemental Figure 4) were measured in sera from mice with B-cell lymphomas, T-cell lymphomas, and other tumors and in sera from tumor-free RzCD19Cre, Rz, CD19Cre, and WT control mice. The levels of these cytokines and chemokines in sera from tumor-bearing RzCD19Cre mice with B-cell lymphomas were not significantly different from those of the control groups, and thus, changes in the expression of these cytokines and chemokines were not strictly correlated with the occurrence of B-cell lymphoma in RzCD19Cre mice.

The levels of amino transferases and sIL-2Rα in mice lacking or harboring B-cell lymphomas

We also examined the levels of AST and ALT in the RzCD19Cre, Rz, CD19Cre, and WT mice. There were no significant differences in the levels of AST and ALT in the sera of mice lacking or harboring B-cell lymphomas ($P > .05$; Figure 4A-B; AST:

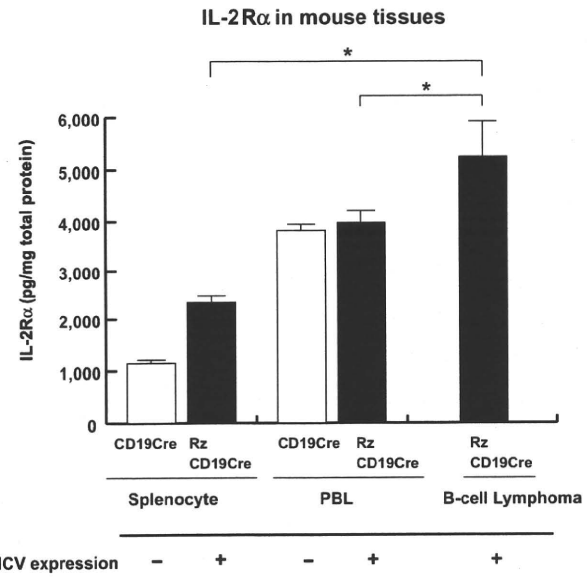

Figure 5. Levels of IL-2Rα in transgenic and control mice lacking or harboring B-cell lymphomas. The expression level of IL-2Rα in splenocytes and PBLs from CD19Cre and RzCD19Cre mice and in B-cell lymphomas from RzCD19Cre mice was measured by ELISA. IL-2Rα levels per total protein are indicated (picograms per milligram). Data from quadruplicate samples are shown as the mean ± SD (*$P < .05$).

RzCD19Cre mice with B-cell lymphomas, 72.2 ± 60.5 IU/L; normal controls, 55.2 ± 23.0 IU/L and ALT: RzCD19Cre mice with B-cell lymphomas, 14.2 ± 3.1 IU/L; normal controls, 11.5 ± 3.0 IU/L).

Finally, we examined the level of sIL-2Rα in the sera of the RzCD19Cre mice with B-cell lymphomas; sIL-2Rα is generated by proteolytic cleavage of IL-2Rα (CD25) residing on the surface of activated T and natural killer cells, monocytes, and certain tumor cells.[24,32] The average sIL-2Rα level in the RzCD19Cre mice with B-cell lymphomas (830.3 ± 533.0 pg/mL) was significantly higher than that in the tumor-free control groups, including the RzCD19Cre, Rz, CD19Cre and WT mice (499.9 ± 110.2 pg/mL; $P < .0057$; Figure 4C). The average sIL-2Rα levels in other tumor-containing groups (430.46 ± 141.15 pg/mL) were not significantly different from those in the tumor-free control groups ($P > .05$; Figure 4C). Moreover, all RzCD19Cre mice with a relatively high level of sIL-2Rα (> 1000 pg/mL) presented with B-cell lymphomas (Figure 4C).

We also examined the level of sIL-2Rα in MxCre/CN2-29 mice and observed a significant increase in sIL-2Rα in mice that expressed HCV and that had B-cell lymphomas compared with tumor-free control (CN2-29) mice (Figure 4D).

Expression of IL-2Rα in B-cell lymphomas of the RzCD19Cre mice

To examine whether sIL-2Rα was derived from lymphoma tissues, we quantified IL-2Rα concentrations in splenocytes, PBLs and B-cell lymphoma tissues (Figure 5). The concentration of IL-2Rα was significantly higher in splenocytes from RzCD19Cre mice compared with those from CD19Cre mice; the concentration was even higher in B-cell lymphoma tissues than in splenocytes from RzCD19Cre mice (Figure 5). These results strongly suggest that B-cell lymphomas directly contribute to the elevated serum concentrations of sIL-2Rα in RzCD19Cre mice.

Discussion

We have established HCV transgenic mice that have a high incidence of spontaneous B-cell lymphomas. In this animal model, the HCV transgene is expressed during the embryonic stage, and these RzCD19Cre mice are expected to be immunotolerant to the HCV transgene product. Thus, the results from this study reveal the potential for the HCV gene to induce B-cell lymphomas without inducing host immune responses against the HCV gene product. A retrospective study indicated that viral elimination reduced the incidence of malignant lymphoma in patients infected with HCV.[33] The results in our study may be consistent with this retrospective observation, indicating the significance of the direct effect of HCV infection on B-cell lymphoma development. Another HCV transgenic mouse strain (MxCre/CN2-29) showed the similarly high incidence of B-cell lymphoma, which strongly supported that development of B-cell lymphomas occurred by the expression of HCV transgene.

Recent findings have revealed the significance of B lymphocytes in HCV infection of liver-derived hepatoma cells.[34] In 4.2% of the RzCD19Cre mice, CD45R-positive intrahepatic lymphomas were identified, and infiltration of B cells into the hepatocytes was frequently observed (data not shown). These phenomena suggest that HCV could modify the in vivo tropism of B cells. The RzCD19Cre mouse is a powerful model system to address these mechanisms in vivo.

As a circulating membrane receptor, sIL-2Rα is localized in lymphoid cells and some other types of cancer cells and is highly expressed in several cancers[35-40] and autoimmune diseases.[41] Recent findings indicate a link between sIL-2Rα levels and hepatocellular carcinoma in Egyptian patients.[42] Appearing on the surface of leukemic cells derived from B and pre-B lymphocytes and other leukemic cells, IL-2Rα is one of the subunits of the IL-2 receptor, which is composed of an α chain (CD25), a β chain (CD122), and a γ chain (CD132).[43] IL-2R ectodomains are thought to be proteolytically cleaved from the cell surface[34,44,45] instead of produced as a result of posttranscriptional splicing.[24] In RzCD19Cre splenocytes, the level of IL-2Rα was higher than that in splenocytes from CD19Cre mice; however, serum concentrations of sIL-2Rα in RzCD19Cre mice without B-cell lymphomas did not show significant differences compared with other control groups (Rz, CD19Cre, and WT). These results indicate the possibility that HCV may increase IL-2Rα expression on B-cells; proteolytic cleavage of IL-2Rα was increased after B-cell lymphoma development in the RzCD19Cre mouse. The detailed mechanism that induces IL-2Rα as a result of HCV expression is still unclear at present, but we have found previously that the HCV core protein induces IL-10 expression in mouse splenocytes.[14] IL-10 up-regulates the expression of IL-2Rα (Tac/CD25) on normal and leukemic B lymphocytes,[46] and therefore, through IL-10, the HCV core protein might induce IL-2Rα in B cells of the RzCD19Cre mouse.

In conclusion, this study established an animal model that will likely provide critical information for the elucidation of molecular mechanism(s) underlying the spontaneous development of B-cell non-Hodgkin lymphoma after HCV infection. This knowledge should lead to therapeutic strategies to prevent the onset and/or progression of B-cell lymphomas.

Acknowledgments

We thank Dr T. Ito for assistance with pathology characterization and Dr T. Munakata for valuable comments.

This work was supported by grants from the Ministry of Health and Welfare of Japan and the Cooperative Research Project on Clinical and Epidemiologic Studies of Emerging and Re-emerging Infectious Diseases.

Authorship

Contribution: K.T.-K. conceived of the project; K.K., M.K., and K.T.-K. designed the studies; Y.K., S.S., M. Saito, K.T., M. Satoh, M.T., and K.T.-K. performed experiments and analyses; N.S. and Y.H. provided scientific advice; and K.T.-K. wrote the manuscript.

Conflict-of-interest disclosure: The authors declare no competing financial interests.

Correspondence: Kyoko Tsukiyama-Kohara, Department of Experimental Phylaxiology, Faculty of Life Sciences, Kumamoto University, Kumamoto 860-8556, Japan; e-mail: kkohara@kumamoto-u.ac.jp.

References

1. Ferri C, Monti M, La Civita L, et al. Infection of peripheral blood mononuclear cells by hepatitis C virus in mixed cryoglobulinemia. *Blood.* 1993; 82(12):3701-3704.
2. Saito I, Miyamura T, Ohbayashi A, et al. Hepatitis C virus infection is associated with the development of hepatocellular carcinoma. *Proc Natl Acad Sci U S A.* 1990;87(17):6547-6549.
3. Simonetti RG, Camma C, Fiorello F, et al. Hepatitis C virus infection as a risk factor for hepatocellular carcinoma in patients with cirrhosis. A case-control study. *Ann Intern Med.* 1992;116(2):97-102.
4. Silvestri F, Pipan C, Barillari G, et al. Prevalence of hepatitis C virus infection in patients with lymphoproliferative disorders. *Blood.* 1996;87(10): 4296-4301.
5. Ascoli V, Lo Coco F, Artini M, Levrero M, Martelli M, Negro F. Extranodal lymphomas associated with hepatitis C virus infection. *Am J Clin Pathol.* 1998;109(5):600-609.
6. Mele A, Pulsoni A, Bianco E, et al. Hepatitis C virus and B-cell non-Hodgkin lymphomas: an Italian multicenter case-control study. *Blood.* 2003; 102(3):996-999.
7. Dammacco F, Sansonno D, Piccoli C, Racanelli V, D'Amore FP, Lauletta G. The lymphoid system in hepatitis C virus infection: autoimmunity, mixed cryoglobulinemia, and overt B-cell malignancy. *Semin Liver Dis.* 2000;20(2):143-157.
8. Gisbert JP, Garcia-Buey L, Pajares JM, Moreno-Otero R. Prevalence of hepatitis C virus infection in B-cell non-Hodgkin's lymphoma: systematic review and meta-analysis. *Gastroenterology.* 2003;125(6):1723-1732.
9. Negri E, Little D, Boiocchi M, La Vecchia C, Franceschi S. B-cell non-Hodgkin's lymphoma and hepatitis C virus infection: a systematic review. *Int J Cancer.* 2004;111(1):1-8.
10. Pileri P, Uematsu Y, Campagnoli S, et al. Binding of hepatitis C virus to CD81. *Science.* 1998; 282(5390):938-941.
11. Rosa D, Saletti G, De Gregorio E, et al. Activation of naive B lymphocytes via CD81, a pathogenetic mechanism for hepatitis C virus-associated B lymphocyte disorders. *Proc Natl Acad Sci U S A.* 2005;102(51):18544-18549.
12. Wakita T, Taya C, Katsume A, et al. Efficient conditional transgene expression in hepatitis C virus cDNA transgenic mice mediated by the Cre/loxP system. *J Biol Chem.* 1998;273(15):9001-9006.
13. Machida K, Tsukiyama-Kohara K, Seike E, et al. Inhibition of cytochrome c release in Fas-mediated signaling pathway in transgenic mice induced to express hepatitis C viral proteins. *J Biol Chem.* 2001;276(15):12140-12146.
14. Machida K, Tsukiyama-Kohara K, Sekiguch S, et al. Hepatitis C virus and disrupted interferon signaling promote lymphoproliferation via type II CD95 and interleukins. *Gastroenterology.* 2009; 137(1):285-296,296 e281-211.
15. Lerat H, Rumin S, Habersetzer F, et al. In vivo tropism of hepatitis C virus genomic sequences in hematopoietic cells: influence of viral load, viral genotype, and cell phenotype. *Blood.* 1998; 91(10):3841-3849.
16. Karavattathayyil SJ, Kalkeri G, Liu HJ, et al. Detection of hepatitis C virus RNA sequences in B-cell non-Hodgkin lymphoma. *Am J Clin Pathol.* 2000;113(3):391-398.
17. Rickert RC, Roes J, Rajewsky K. B lymphocyte-specific, Cre-mediated mutagenesis in mice. *Nucleic Acids Res.* 1997;25(6):1317-1318.
18. Tanaka T, Lau JY, Mizokami M, et al. Simple fluorescent enzyme immunoassay for detection and quantification of hepatitis C viremia. *J Hepatol.* 1995;23(6):742-745.
19. Tsukiyama-Kohara K, Tone S, Maruyama I, et al. Activation of the CKI-CDK-Rb-E2F pathway in full genome hepatitis C virus-expressing cells. *J Biol Chem.* 2004;279(15):14531-14541.
20. Nishimura T, Kohara M, Izumi K, et al. Hepatitis C virus impairs p53 via persistent overexpression of 3beta-hydroxysterol Delta24-reductase. *J Biol Chem.* 2009;284(52):36442-36452.
21. Tsukiyama-Kohara K, Poulin F, Kohara M, et al. Adipose tissue reduction in mice lacking the translational inhibitor 4E-BP1. *Nat Med.* 2001; 7(10):1128-1132.
22. Fujimura S, Xing Y, Takeya M, et al. Increased expression of germinal center-associated nuclear protein RNA-primase is associated with lymphomagenesis. *Cancer Res.* 2005;65(13):5925-5934.
23. Miyazaki T, Kato I, Takeshita S, Karasuyama H, Kudo A. Lambda5 is required for rearrangement of the Ig kappa light chain gene in pro-B cell lines. *Int Immunol.* 1999;11(8):1195-1202.
24. Rubin LA, Galli F, Greene WC, Nelson DL, Jay G. The molecular basis for the generation of the human soluble interleukin 2 receptor. *Cytokine.* 1990;2(5):330-336.
25. Tsukiyama-Kohara K, Iizuka N, Kohara M, Nomoto A. Internal ribosome entry site within hepatitis C virus RNA. *J Virol.* 1992;66(3):1476-1483.
26. Jaffe ES, Harris NL, Stein H, Isaacson PG. Classification of lymphoid neoplasms: the microscope as a tool for disease discovery. *Blood.* 2008; 112(12):4384-4399.
27. el-Din HM, Attia MA, Hamza MR, Khaled HM, Thoraya MA, Eisa SA. Hepatitis C Virus and related changes in immunologic parameters in non Hodgkin's lymphoma patients. *Egypt J Immunol.* 2004;11(1):55-64.
28. Feldmann G, Nischalke HD, Nattermann J, et al. Induction of interleukin-6 by hepatitis C virus core protein in hepatitis C-associated mixed cryoglobulinemia and B-cell non-Hodgkin's lymphoma. *Clin Cancer Res.* 2006;12(15):4491-4498.
29. Mizuochi T, Ito M, Takai K, Yamaguchi K. Differential susceptibility of peripheral blood CD5+ and CD5− B cells to apoptosis in chronic hepatitis C patients. *Biochem Biophys Res Commun.* 2009; 389(3):512-515.
30. Bansal AS, Bruce J, Hogan PG, Prichard P, Powell EE. Serum soluble CD23 but not IL8, IL10, GM-CSF, or IFN-gamma is elevated in patients with hepatitis C infection. *Clin Immunol Immunopathol.* 1997;84(2):139-144.
31. Barrett L, Gallant M, Howley C, et al. Enhanced IL-10 production in response to hepatitis C virus proteins by peripheral blood mononuclear cells from human immunodeficiency virus-monoinfected individuals. *BMC Immunol.* 2008;9:28.
32. Rubin LA, Kurman CC, Fritz ME, et al. Soluble interleukin 2 receptors are released from activated human lymphoid cells in vitro. *J Immunol.* 1985;135(5):3172-3177.
33. Kawamura Y, Ikeda K, Arase Y, et al. Viral elimination reduces incidence of malignant lymphoma in patients with hepatitis C. *Am J Med.* 2007; 120(12):1034-1041.
34. Stamataki Z, Shannon-Lowe C, Shaw J, et al. Hepatitis C virus association with peripheral blood B lymphocytes potentiates viral infection of liver-derived hepatoma cells. *Blood.* 2009;113(3): 585-593.
35. Wasik MA, Sioutos N, Tuttle M, Butmarc JR, Kaplan WD, Kadin ME. Constitutive secretion of soluble interleukin-2 receptor by human T cell lymphoma xenografted into SCID mice. Correlation of tumor volume with concentration of tumor-derived soluble interleukin-2 receptor in body fluids of the host mice. *Am J Pathol.* 1994;144(5): 1089-1097.
36. Tsai MH, Chiou SH, Chow KC. Effect of platelet activating factor and butyrate on the expression of interleukin-2 receptor alpha in nasopharyngeal carcinoma cells. *Int J Oncol.* 2001;19(5):1049-1055.
37. Yano T, Yoshino I, Yokoyama H, et al. The clinical significance of serum soluble interleukin-2 receptors in lung cancer. *Lung Cancer.* 1996;15(1):79-84.
38. Tesarova P, Kvasnicka J, Umlaufova A, Homolkova H, Jirsa M, Tesar V. Soluble TNF and IL-2 receptors in patients with breast cancer. *Med Sci Monit.* 2000;6(4):661-667.
39. Maccio A, Lai P, Santona MC, Pagliara L, Melis GB, Mantovani G. High serum levels of soluble IL-2 receptor, cytokines, and C reactive protein correlate with impairment of T cell response in patients with advanced epithelial ovarian cancer. *Gynecol Oncol.* 1998;69(3):248-252.
40. Matsumoto T, Furukawa A, Sumiyoshi Y, Akiyama KY, Kanayama HO, Kagawa S. Serum levels of soluble interleukin-2 receptor in renal cell carcinoma. *Urology.* 1998;51(1):145-149.
41. Pountain G, Hazleman B, Cawston TE. Circulating levels of IL-1beta, IL-6 and soluble IL-2 receptor in polymyalgia rheumatica and giant cell arteritis and rheumatoid arthritis. *Br J Rheumatol.* 1998;37(7):797-798.
42. Zekri AR, Alam El-Din HM, Bahnassy AA, et al. Serum levels of soluble Fas, soluble tumor necrosis factor-receptor II, interleukin-2 receptor and interleukin-8 as early predictors of hepatocellular carcinoma in Egyptian patients with hepatitis C virus genotype-4. *Comp Hepatol.* 2010:9(1):1.
43. Sheibani K, Winberg CD, van de Velde S, Blayney DW, Rappaport H. Distribution of lymphocytes with interleukin-2 receptors (TAC antigens) in reactive lymphoproliferative processes, Hodgkin's disease, and non-Hodgkin's lymphomas. An immunohistologic study of 300 cases. *Am J Pathol.* 1987;127(1):27-37.
44. Robb RJ, Rusk CM. High and low affinity receptors for interleukin 2: implications of pronase, phorbol ester, and cell membrane studies upon the basis for differential ligand affinities. *J Immunol.* 1986;137(1):142-149.
45. Sheu BC, Hsu SM, Ho HN, Lien HC, Huang SC, Lin RH. A novel role of metalloproteinase in cancer-mediated immunosuppression. *Cancer Res.* 2001;61(1):237-242.
46. Fluckiger AC, Garrone P, Durand I, Galizzi JP, Banchereau J. Interleukin 10 (IL-10) up-regulates functional high affinity IL-2 receptors on normal and leukemic B lymphocytes. *J Exp Med.* 1993; 178(5):1473-1481.

JOURNAL OF CLINICAL MICROBIOLOGY, Nov. 2010, p. 3843–3851 Vol. 48, No. 11
0095-1137/10/$12.00 doi:10.1128/JCM.00415-10

Detection of Hepatitis B and C Viruses in Almost All Hepatocytes by Modified PCR-Based *In Situ* Hybridization▽

Hideko Nuriya,[1] Kazuaki Inoue,[1,2] Takeshi Tanaka,[3] Yukiko Hayashi,[4] Tsunekazu Hishima,[4] Nobuaki Funata,[4] Kyosuke Kaji,[5] Seishu Hayashi,[3] Shuichi Kaneko,[5] and Michinori Kohara[1]*

Department of Microbiology and Cell Biology, Tokyo Metropolitan Institute of Medical Science, 2-1-6 Kamikitazawa, Setagaya-ku, Tokyo 156-0057, Japan[1]; Division of Gastroenterology, Showa University Fujigaoka Hospital, 1-30 Aoba-ku, Fujigaoka, Yokohama 227-8501, Japan[2]; Liver Unit, Tokyo Metropolitan Komagome Hospital, 3-18-22 Honkomagome, Bunkyo-ku, Tokyo 113-8613, Japan[3]; Department of Pathology, Tokyo Metropolitan Komagome Hospital, 3-18-22 Honkomagome, Bunkyo-ku, Tokyo 113-8613, Japan[4]; and Department of Gastroenterology, Kanazawa University Graduate School of Medical Science, Ishikawa 920-8641, Japan[5]

Received 28 February 2010/Returned for modification 22 April 2010/Accepted 16 August 2010

Although PCR-based *in situ* hybridization (PCR-ISH) can be used to determine the distribution and localization of pathogens in tissues, this approach is hampered by its low specificity. Therefore, we used a highly specific and sensitive PCR-ISH method to reveal the lobular distribution and intracellular localization of hepatitis B virus (HBV) and HCV in chronic liver disease and to clarify the state of persistent HBV and HCV infection in the liver. HBV genomic DNA was detected in almost all hepatocytes, whereas HBV RNA or protein was differentially distributed only in a subset of the HBV DNA-positive region. Further, HCV genomic RNA was detected in almost all hepatocytes and was localized to the cytoplasm. HCV RNA was also detected in the epithelium of the large bile duct but not in endothelial cells, portal tracts, or sinusoidal lymphocytes. In patients with HBV and HCV coinfection, HCV RNA was localized to the noncancerous tissue, whereas HBV DNA was found only in the cancerous tissue. Using this novel PCR-ISH method, we could visualize the staining pattern of HBV and HCV in liver sections, and we obtained results consistent with those of real-time detection (RTD)-PCR analysis. In conclusion, almost all hepatocytes are infected with HBV or HCV in chronic liver disease; this finding implies that the viruses spreads throughout the liver in the chronic stage.

Hepatitis B virus (HBV) and hepatitis C virus (HCV) are the primary causative agents of chronic liver disease (2, 9, 17). HBV infection remains a global health problem; it is estimated that 350 million individuals are persistently infected with the virus and that approximately 15% to 25% of these individuals will die due to the sequelae of the infection (23, 29). Further, more than 170 million people are infected with HCV worldwide (21). HCV has a single-stranded RNA genome (8, 19), does not have canonical oncogenes, and can easily establish chronic infection without integration into the host genome (3, 20), resulting in hepatic steatosis and hepatocellular carcinoma (HCC) (28). The viruses share a similar route of transmission, such as via the transfusion of infected blood or body fluids or use of contaminated needles.

Several studies have shown that 10% to 35% of the individuals infected with HBV also have HCV infection, although the prevalence varies depending on the population studied (4, 32, 34). The relationship between coinfection and acceleration of malignant transformation remains unclear, but HBV and HCV coinfection seems to alter the natural history of both HBV-related and HCV-related liver disease (2, 12). HCV has been shown to inhibit HBV gene expression (7, 15). The high prevalence of occult HBV infection may indicate that HCV also inhibits HBV replication (34). Most epidemiological studies of HBV have been performed by using diagnostic serological assays (16). We recently used a novel, highly sensitive diagnostic PCR method to demonstrate that the HBV genome is detectable in the sera of a substantial proportion of patients with chronic HCV infection who are seronegative for the standard HBV-related markers (1, 34). Further, we reported the levels of HBV DNA and HCV RNA in cancerous and noncancerous liver tissue using real-time detection (RTD)-PCR (34). RTD-PCR is an accurate assay method, but it can determine the levels of genomic DNA and RNA only in homogenized tissue. In this study, we developed a PCR-based *in situ* hybridization (PCR-ISH) method for detecting and visualizing HBV DNA, HBV RNA, and HCV RNA and comparing their protein expression patterns, with the aim to reveal the lobular distribution and intracellular localization of HBV and HCV in chronic liver disease and to clarify the state of persistent HBV and HCV infection in the liver.

MATERIALS AND METHODS

Patients. Twenty-nine patients were admitted to Tokyo Metropolitan Komagome Hospital for the treatment of hepatic tumors. Of these patients, 14 were considered to have chronic HCV infection (persistently positive results for HCV antibody), 8 were diagnosed with chronic hepatitis B (persistently positive results for HBV surface antigen [HBsAg]), and 7 showed negative results for both viral markers but had metastatic liver cancer (6 with colonic cancer and 1 with gastric cancer). We used four samples from seven patients as controls for PCR-ISH and four samples from seven patients as controls for reverse transcriptase PCR (RT-PCR)–ISH (Table 1). Of the 14 patients with chronic hepatitis C, two showed positive results for HBV DNA by RTD-PCR. HBsAg and second-generation HCV antibody were measured by using enzyme-linked immunosor-

* Corresponding author. Mailing address: Department of Microbiology and Cell Biology, The Tokyo Metropolitan Institute of Medical Science, 2-1-6, Kamikitazawa, Setagaya-ku, Tokyo 156-8506, Japan. Phone: 81-3-5316-3232. Fax: 81-3-5316-3137. E-mail: kohara-mc@igakuken.or.jp.

▽ Published ahead of print on 25 August 2010.

TABLE 1. Patient profiles and results of the present study

Patient no.	Age (yr)	Gender[a]	HCV antibody	HBs Ag	Liver histology	RT-PCR–ISH HCV	PCR-ISH HBV	Serum HBV DNA (copies/ml)[b]	Serum HCV RNA		IFN treatment	Note
									Copies/ml	KIU/ml[d]		
1	53	M	−	+	A2F3		+	1.1×10^2			−	
2	42	M	−	+	A2F2		+	4.0×10^5			−	Fig. 2A
3	43	M	−	+	A2F3		+	1.6×10^7			−	
4	53	M	−	+	A2F4		+	6.4×10^3			−	Fig. 1A
5	55	M	−	+	A2F3		+	1.0×10^3			−	Fig. 3A
6	54	M	−	+	A2F4	−	+	NT[c]			−	
7	31	M	−	+	A3F3		+	3.0×10^9			+	
8	61	F	−	+	A3F3		+	NT			−	
9	63	M	+	−	A3F4	+	−		5.6×10^6		−	Fig. 4D
10	56	M	+	−	A2F3	+	−		NT		+	
11	67	F	+	−	A3F4	−	−		NT		−	
12	73	M	+	−	A2F4	+			1.2×10^6		−	Fig. 1B
13	68	F	+	−	A3F4	+			1.1×10^6		−	
14	76	F	+	−	A2F4	+			9.5×10^5		−	Fig. 4A
15	62	M	+	−	A2F3	+			7.2×10^5		−	
16	65	M	+	−	A3F4	+			NT		−	
17	60	F	+	−	A3F4	+				41	−	
18	48	F	+	−	A2F1	+			7.6×10^6	>850	−	Fig. 4C
19	43	M	+	−	A2F3	+				389	−	
20	59	M	+	−	A2F3	+				>850	−	
21	72	F	+	−	A2F4	+	+	3.9×10^1	5.0×10^7			Fig. 5
22	69	M	+	−	A2F3	+	+	5.0×10^1	3.0×10^7			
23	69	M	−	−	Normal	−	−					Gastric cancer
24	58	M	−	−	Normal		−					Colon cancer
25	58	M	−	−	Normal	−						Colon cancer
26	59	F	−	−	Normal	−						Colon cancer
27	65	M	−	−	Normal	−						Colon cancer
28	47	M	−	−	Normal		−					Colon cancer
29	81	F	−	−	Normal		−					Colon cancer

[a] M, male; F, female.
[b] Serum HBV DNA was positive in patients 21 and 22.
[c] NT, not tested.
[d] KIU, kilo international units.

bent assay (ELISA) kits (Abbott Laboratories, Chicago, IL, and International Reagent Corp., Kobe, Japan, respectively). All 29 patients underwent hepatic resection. Histological evaluation of the liver was carried out according to the METAVIR scoring system (3).

Ethical approval. The Institutional Review Board of Tokyo Metropolitan Komagome Hospital approved the study. Written informed consent was obtained from all the subjects.

Sample preparation. The liver tissue samples for HBV DNA detection were fixed in 10% buffered formalin (pH 7.4) for 18 h, embedded in paraffin, cut into 6-μm-thick sections, and mounted on silane-coated glass slides for use with a GeneAmp *in situ* PCR system 1000 unit (Applied Biosystems, Foster City, CA). The slides were washed thrice in xylene for 8 min at each washing, rinsed thrice in 99.5% ethanol and 75% ethanol for 5 min at each rinsing, and rehydrated in distilled water for deparaffinization. For detecting HBV mRNA and HCV RNA, OCT-embedded frozen liver tissue samples were cut into 10-μm-thick sections and mounted on silane-coated glass slides. They were then fixed in 10% buffered formalin (pH 7.4) for 17 to 21 h, rinsed twice in distilled water treated with 0.01% diethylpyrocarbonate (DEPC) for 2 min at each rinse, rinsed in 99.5% ethanol for 1 min, and then air dried and stored at −80°C until use. The tissue sections on the glass slides were digested with proteinase K (1 to 30 μg/ml and 1 to 200 μg/ml for the noncancerous and cancerous regions of the paraffin-embedded sections, respectively; 0.008 to 1.0 μg/ml for the frozen sections) in 50 mM Tris (pH 7.5) at 37°C for 30 min in a humidified chamber. Subsequently, proteinase K was inactivated at 97°C for 10 min, and then the sections were rinsed with distilled water, dehydrated in 99.5% ethanol, and air dried.

Primers and probes for PCR-ISH and RT-PCR–ISH. The primers used to amplify the S and X regions of HBV and the 5′ untranslated region (5′-UTR) of HCV as well as the corresponding probes are listed in Table 2. We created a digoxigenin (DIG)-dUTP tail at the 3′ end of the 5′-DIG probe using a DNA tailing kit (Roche, Basel, Switzerland).

PCR-ISH for detecting HBV DNA. PCR was performed by using one of two sets of antisense and sense primers complementary to the sequences located in the S and X regions of HBV. The PCR mixture contained 10 mM Tris-HCl (pH 8.3), 50 mM KCl, 3.0 mM $MgCl_2$, 0.8 mM each primer, 197 mM deoxynucleoside triphosphates (dNTPs), and 10 U/50 μl *Taq* DNA polymerase (AmpliTaq Gold; Applied Biosystems).

The tissue slides were warmed to 70°C, and 50 μl of the PCR mixture was overlaid onto the proteinase K-treated tissue specimens. An Ampli cover disc with Ampli cover clips (Applied Biosystems) was attached to each specimen. The slides were placed in the GeneAmp *in situ* PCR system 1000 unit at 70°C. PCR was performed at 95°C for 10 min, followed by 35 to 55 cycles at 95°C for 30 s and 60°C for 2 min and a final extension at 72°C for 10 min. Immediately after the PCR, the slides were fixed in 4% paraformaldehyde in phosphate-buffered saline (PBS) for 10 min at 37°C, washed in 2× SSC (1× SSC is 0.15 M NaCl plus 0.015 M sodium citrate) for 2 min, rinsed with distilled water for 2 min, dehydrated in 99.5% ethanol for 1 min, and then air dried. ISH was performed by mixing the DIG-labeled probe (final concentration, 100 ng/ml) with 65 μl of hybridization buffer (50% deionized formamide, 4× SSC, 1× Denhardt's solution [0.2% bovine serum albumin {BSA}, 0.2% polyvinyl pyrrolidone, 0.2% Ficoll 400], 100 μg/ml denatured salmon sperm DNA, 100 μg/ml yeast RNA, and 1 mM EDTA) and then adding the mixture to each section, heating to 97°C for 10 min, and cooling to 37°C in decrements of 1°C/min (27). Hybridization was carried out overnight at 37°C. Stringency washes were conducted with the following: 2× SSC twice for 10 min at 37°C, 0.03× SSC for 10 min at 50°C, 0.1% Triton X-100 in TBS (0.1 M Tris [pH 7.5], 0.1 M NaCl) for 10 min at room temperature, and TBS for 5 min at room temperature. After incubation in blocking reagent (0.1 M Tris

[pH 7.5], 0.1 M NaCl, 10% sheep serum, 3% BSA) at room temperature for 15 min, the slides were covered with 100 μl anti-DIG antibody conjugated with alkaline phosphatase (Roche) and diluted at 1:900 with 1% BSA in TBS at 37°C for 60 min. After this reaction, the slides were washed twice (3 min each) with 0.1% Triton X-100 in TBS, then with TBS alone, and finally with APS (0.1 M Tris [pH 9.0], 0.1 M NaCl, 50 mM $MgCl_2$) at room temperature. The slides were incubated in 100 μl dye solution (338 μg/ml nitroblue tetrazolium chloride [NBT], 175 μg/ml 5-bromo-4-chloro-3-indolyl-phosphate 4-toluidine salt [BCIP], and 450 μM Levamisole [Vector Labs, Burlingame, CA] in APS) at 37°C in the dark. After sufficient color development, they were washed with deionized water for 1 min and then mounted with aqueous mounting medium.

RT-PCR–ISH for detecting HBV RNA. The OCT-embedded frozen sections were placed on glass slides. After proteinase K treatment, the tissue sections were digested with RNase-free DNase I (Roche; diluted to 3 U/μl in 0.1 M sodium acetate and 5 mM $MgSO_4$). The DNase I reaction mixture (66 μl) was overlaid onto the tissue sections, which were then enclosed in a frame. The slides were reacted in an aluminum box at 37°C for 20 min and inactivated at 97°C for 10 min. They were then washed in DEPC-treated water, dehydrated in 99.5% ethanol, and air dried.

Moloney murine leukemia virus (MMLV) reverse transcriptase (10 U/μl; Invitrogen, Carlsbad, CA) was used in a reaction mixture containing 10 mM Tris-HCl (pH 8.3), 50 mM KCl, 5.0 mM $MgCl_2$, 1 μM antisense primer, 1 mM dNTPs, 2 U/μl RNase inhibitor (Takara, Otsu, Japan), and 10 mM dithiothreitol (DTT). The specimens were then overlaid with the mixture, reacted at 42°C for 60 min, washed with distilled water, dehydrated in 99.5% ethanol, and air dried. The subsequent procedures were the same as described for PCR-ISH.

Immunohistochemical staining for detecting HBV proteins. Deparaffinized formaldehyde-fixed sections or fixed frozen liver tissue sections on glass slides were soaked in distilled water, digested with 0.1% pronase (protease P8038 XXIV; Sigma-Aldrich, Tokyo, Japan) for 1 min, and washed with PBS at room temperature. After 30 min of incubation in blocking reagent (1% BSA and 2.5 mM EDTA in PBS) at room temperature, the slides were reacted with 100 μl of anti-HBs and anti-HBc polyclonal antibody solutions for 3 h at room temperature and then overnight at 4°C. The following polyclonal antibodies were used: anti-HBs rabbit polyclonal antibody anti-HBc rabbit polyclonal antibody (Novocastra Laboratories, Newcastle, United Kingdom), or normal rabbit serum diluted in blocking reagent. After the reaction, the slides were washed four times with PBS at room temperature and incubated for 60 min at room temperature in 100 μl anti-rabbit IgG conjugated with peroxidase (Amersham ECL; GE Healthcare, Piscataway, NJ) diluted to 1:100 in blocking reagent. The slides were then washed four times with PBS at room temperature and stained by using 3,3′-diaminobenzidine tetrahydrochloride (DAB) (Vector Labs). Following counterstaining with Mayer's hematoxylin solution, the tissue specimens were dehydrated in 99.5% ethanol and 80% xylene. The slides were sealed by using Bioleit (Oken Shoji, Tokyo, Japan).

RT-PCR–ISH for detecting HCV RNA. HCV RNA was detected by using methods similar to those used for detecting HBV RNA except for the following steps: the DNase I step was omitted, and 1.5 mM $MgCl_2$ was used in the PCR mixture.

Primers and probe sets in RTD-PCR for quantifying HBV DNA, HCV RNA, β-actin DNA, and GAPDH mRNA. The primer sets to quantify the S and X regions of HBV were the same as those used for PCR-ISH. The TaqMan probes for these regions, the primers and probe designed to quantify the 5′-UTR of HCV (33), and those used to quantify β-actin genomic DNA and GAPDH (glyceraldehyde-3-phosphate dehydrogenase) mRNA (internal control) are shown in Table 2. Each PCR comprised 50 cycles (95°C for 30 s, 60°C for 40 s, and 72°C for 30 s) in a real-time PCR system (ABI Prism 7700 sequence detector system; Applied Biosystems).

Amplicor monitor assays. The Amplicor monitor assays were performed as described previously (22, 24, 33, 36).

HE staining. HBV- or HCV-infected deparaffinized formaldehyde-fixed sections or fixed frozen liver tissue sections were stained with hematoxylin and eosin (HE).

LCM of liver tissue. A frozen liver tissue sample was sectioned by using a cryostat and fixed in acetone, followed by HE staining. Laser capture microdissection (LCM) was performed by using an LM 200 system (Olympus, Tokyo, Japan) as described previously (6, 11). This procedure produced approximately 30 hepatocytes from each of three areas (perivenular, intermediate, and periportal) in the section. Total RNA was extracted from the LCM samples, and HCV RNA and GAPDH mRNA were quantified by RTD-PCR.

TABLE 2. Primers and probes for PCR-ISH and RT-PCR

Technique	Virus or protein (region)	Primer or probe		
		Type	Description, nucleotides	Sequence
PCR-ISH	HBV (HBs)	Primer	Forward (HB-166-S21), 166–186	5′-CACATCAGGATTCCTAGGACC-3′
			Reverse (HB-344-R20), 344–325	5′-AGGTTGGTGAGTGATTGGAG-3′
		Probe	(HB-242-S45D), 242–286	5′-(DIG)-CAGAGTCTAGACTCGTGGTGGACTTCTCTCAATTTTCTAGGGGGA-(DIG)n-3′
	HBV (HBx)	Primer	Forward (HB-1584-S21), 1584–1604	5′-CTTCGCTTCACCTCTGCACGT-3′
			Reverse (HB-1744-R23), 1744–1722	5′-CCCAACTCCTCCCAGTCCTTAAA-3′
		Probe	(HB-1705-R45D), 1705–1661	5′-(DIG)-TATGCCTCAAGGTCGGTCGTTGACATTGCTGAGAGTCCAAGAGTC-(DIG)n-3′
RT-PCR–ISH	HCV (5′-UTR)	Primer	Forward (R6-129-S19), 129–147	5′-CCGGGAGAGCCATAGTGGT-3′
			Reverse (R6-290-R19), 290–272	5′-AGTACCACAAGGCCTTTCG-3′
		Probe	(R6-225-S45D), 225–269	5′-(DIG)-ATTTGGGCGTGCCCCCGCGAGACTGCTAGCCGAGTAGTGTTGGGT-(DIG)n-3′
TaqMan	HBV (S)	Probe	Forward (HB-242-S26FT), 242–267	5′-CAGAGTCTAGACTCGTGGTGGACTTC-3′
	HBV (X)	Probe	Forward (HB-1681-S25FT), 1681–1705	5′-TGTCAACGACCGACCTTGAGGCATA-3′
	HCV (5′-UTR)	Primer	Forward (R6-130-S17), 130–146	5′-CGGGAGAGCCATAGTGG-3′
			Reverse (R6-290-R19), 290–272	5′-AGTACCACAAGGCCTTTCG-3′
		Probe	Forward (R6-148-S21FT), 148–168	5′-CTGCGGAACCGGTGAGTACAC-3′
	β-Actin (genomic DNA)	Primer	Forward (β-ACT-1998-S20), 1998–2017	5′-CAGTGTGACATGGTGCATCT-3′
			Reverse (β-ACT-2246-R24), 2246–2223	5′-GTGAGGATCTTCATGAGGTAGTCA-3′
		Probe	Forward (β-ACT-2063-S22FT), 2063–2084	5′-ACGTTGCTATCCAGGCTGTGCT-3′
	GAPDH	Primer	Forward (GAPDH-514-S24), 514–537	5′-TGCACCACCAACTGCTTAGCACCC-3′
			Reverse (GAPDH-837-R24), 837–814	5′-CTTGATGTCATCATATTTGGCAGG-3′
		Probe	Forward (GAPDH-584-S25FT), 584–608	5′-TGACCACAGTCCATGCCATCACTGC-3′

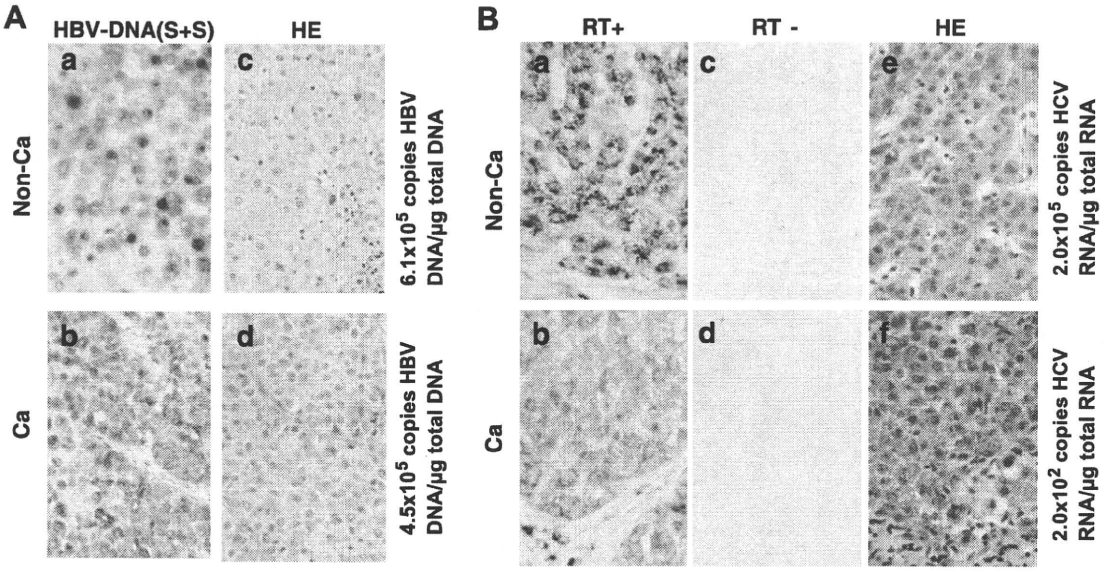

FIG. 1. (A) Panels a and b, HBV DNA detected by PCR-ISH and immunohistochemical staining in noncancerous (Non-Ca) (panel a) and cancerous (Ca) (panel b) liver tissues obtained from a patient infected with HBV. The numbers of PCR cycles were 37 and 42, respectively. Panels c and d, serial sections were stained with HE. Magnification, ×400. S+S, primers and probe targeting the S region of HBV DNA. (B) Panels a and b, HCV RNA detected by RT-PCR–ISH (45 cycles of PCR) in noncancerous (panel a) and cancerous (panel b) tissues obtained from a patient infected with HCV. Panels c and d, no HCV RNA was detected in the RT-negative controls. Panels e and f, serial sections were stained with HE. Magnification, ×400.

RESULTS

Sensitivity and specificity of PCR-ISH versus RTD-PCR for detecting HBV DNA and HCV RNA. PCR-ISH showed positive results for HBV DNA in 10 tissue specimens from eight HBsAg-seropositive patients and two patients whose serum HBV DNA was barely detected by RTD-PCR despite being their HBsAg negative (patients 21 and 22) (Table 1). PCR-ISH yielded negative results for four patients who were negative for serum HBsAg and HCV antibody (patients 23, 24, 28, and 29) and three patients who were negative for serum HBsAg but positive for HCV antibody (patients 9 to 11).

Thirteen of the 14 tissue specimens from the patients with serum HCV antibody had a positive result for HCV RNA by RT-PCR–ISH (sensitivity, 92.9%). In contrast, HCV RNA was not detected by RT-PCR–ISH in four tissue specimens from the patients negative for both HCV antibody and HBsAg (patients 23, 25, 26, and 27) or in the sample from an HBsAg-positive and HCV antibody-negative patient (patient 6).

We performed PCR-ISH and RT-PCR–ISH on the same HBV- or HCV-infected samples from noncancerous and cancerous regions in which we had previously quantitated viral genomic DNA or RNA by RTD-PCR (34). The noncancerous tissue contained 6.1×10^5 copies of HBV DNA/μg total DNA, and the cancerous regions included 4.5×10^5 copies/μg total DNA. Equivalent numbers of cells in the noncancerous and cancerous tissues stained positive for HBV on PCR-ISH (patient 4; Fig. 1A). The PCR-ISH results were consistent with the HBV DNA copy number previously determined by RTD-PCR (34).

Noncancerous tissue from an HCV-positive patient contained 2.0×10^5 copies HCV RNA/μg total RNA, whereas cancerous tissue contained 2.0×10^2 copies/μg total RNA (patient 12; Fig. 1B). HCV RNA was observed by RT-PCR–ISH in hepatocytes of the liver tissue sections from an HCV-infected patient (Fig. 1B). In the noncancerous tissue, an intense hybridization signal was found at the perinuclear sites of almost all the hepatocytes in the section (Fig. 1B, panel a). In contrast, in the cancerous tissue, there was only a weak HCV RNA hybridization signal in the hepatocytes (Fig. 1B, panel b). When the RT step was omitted (control), no HCV RNA was detected in the noncancerous or cancerous tissue sections (Fig. 1B, panels c and d). These results were consistent with the previous quantitation of HCV RNA copy number by RTD-PCR (34).

Detection of HBV DNA by PCR-ISH. HBV DNA was detected by PCR-ISH in the tissue sections obtained from an HBV DNA-seropositive patient. Amplified PCR products were detected by using a probe for either the S or the X region (Fig. 2A, panels a to d) but were not detected by using a heterologous probe (Fig. 2A, panels e and f). Amplification of either the S or the X region of HBV DNA gave the same pattern of hybridization (Fig. 2A, panels a to d). HBV DNA was detected by PCR-ISH in almost all hepatocytes (Fig. 2A, panels a to d) and was very obvious even under low magnification (Fig. 2A, panels a and c). An intense hybridization signal was observed predominantly at the perinuclear site under high magnification (Fig. 2A, panels b and d). In contrast, HBV DNA was not detected by using HBs- and HBx-matched primer and probe combinations in sections obtained from an HBV DNA-seronegative patient (data not shown). DNA fragments amplified by using the S and X region primer sets were 179 bp and 161 bp, respectively (Fig. 2B). Sections from an HBV DNA-seronegative patient were negative in the PCR analysis (data not shown).

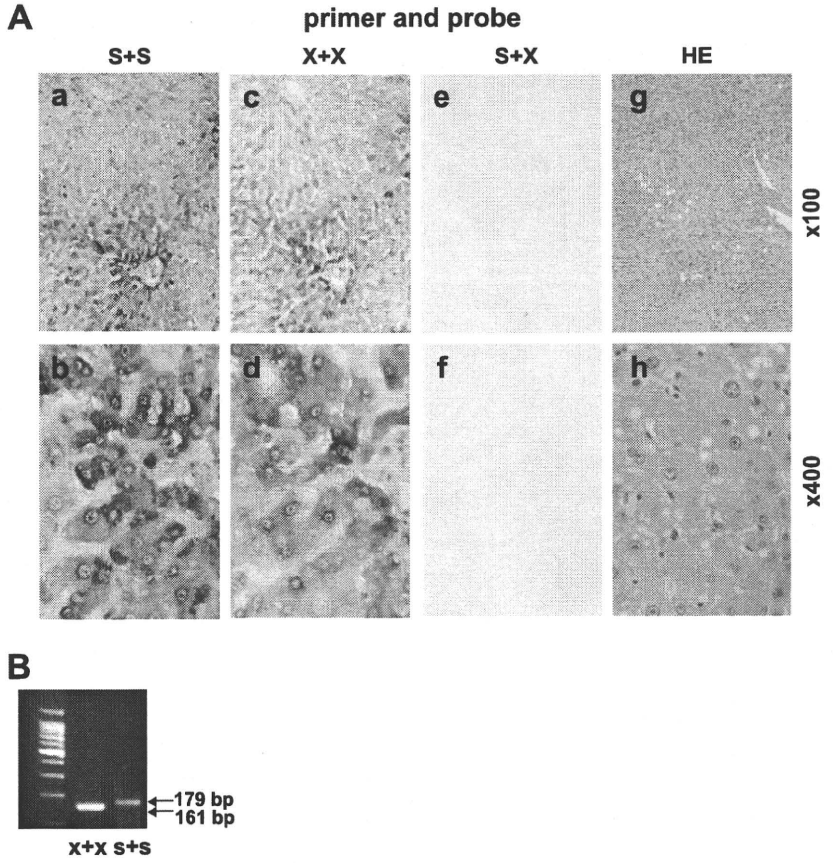

FIG. 2. (A) Panels a to f, HBV DNA detected in liver tissue sections from a patient with chronic hepatitis B by PCR-ISH (42 cycles of PCR). Panels g and h, serial sections were stained with HE. Magnifications, ×100 (panels a, c, e, and g) and ×400 (b, d, f, and h). S+S, primers and probe targeting the S region; X+X, primers and probe targeting the X region; S+X, primers and probe targeting the S and X regions, respectively. (B) Amplified DNA fragments in the PCR mixture of the section in panel A visualized by 3% agarose gel electrophoresis. The PCR product of the X region was 161 bp, and that of the S region was 179 bp.

Localization of HBV DNA, HBV RNA, HBsAg, and HBcAg in liver tissue. HBV DNA, HBV RNA, HBsAg, and HBcAg were detected by PCR-ISH, RT-PCR–ISH, and immunohistochemical staining of serial sections from an HBV-infected patient (patient 5; Fig. 3A, panels a to h). HBV DNA was detected in almost all the hepatocytes by PCR-ISH, although there was wide variation in the hybridization signal intensity between different areas of the section (Fig. 3A, panels a and b). The staining pattern of HBV RNA was similar to that of HBV DNA (Fig. 3A, panels c and d). Intracytoplasmic and intranuclear staining for HBsAg and HBcAg, respectively, was found in some hepatocytes (Fig. 3A, panels f and h). PCR and RT-PCR results were confirmed by gel electrophoresis of the amplified products in the supernatant from the tissue section (Fig. 3B, panels a and b).

Detection of HCV RNA by RT-PCR–ISH. HCV RNA could be detected by RT-PCR–ISH in almost all the hepatocytes in the liver sections obtained from an HCV RNA-seropositive patient (Fig. 4A, panels a and b). Under high magnification, a strong HCV RNA signal was detected in the perinuclear area (Fig. 4A, panel b). A negative-control test (no RT) did not detect any HCV RNA (Fig. 4A, panels c and d). The expected 162-bp DNA fragment amplified by RT-PCR in the supernatant from the tissue section was detected (Fig. 4B, lane 2). In contrast, HCV RNA was not detected in the liver section obtained from an HCV RNA-seronegative patient, regardless of whether RT was used (data not shown).

Isolation of HCV RNA in hepatocytes by LCM. Hepatocyte groups were captured from the perivenular, intermediate, and periportal areas by LCM (Fig. 4C, panel a). HCV RNA was quantified by RTD-PCR in approximately 30 hepatocytes captured by LCM and normalized against the picogram weight of GAPDH mRNA (Fig. 4C, panels b to d); the HCV RNA levels were equivalent in all three regions (Fig. 4C, panel d).

Detection of HCV RNA in the epithelium of the large bile duct. HCV RNA was detected by RT-PCR–ISH in the epithelium of the large bile duct, which was surrounded by dense fibrous and elastic tissue (Fig. 4D, panels a and b). In contrast, no HCV RNA was detected in the epithelium of the small bile duct. Further, HCV RNA was not detected in the portal vein or its branches (Fig. 4D, panel a).

Detection of HBV DNA and HCV RNA in noncancerous and cancerous liver tissue sections obtained from a patient with HBV and HCV coinfection. Figure 5 shows the results for HBV DNA and HCV RNA in liver samples from a patient with HCC having HCV and HBV coinfection. The amounts of serum HBV DNA and HCV RNA were 39 copies/ml and 5×10^7 copies/ml, respectively (patient 21) (34). In the noncancerous

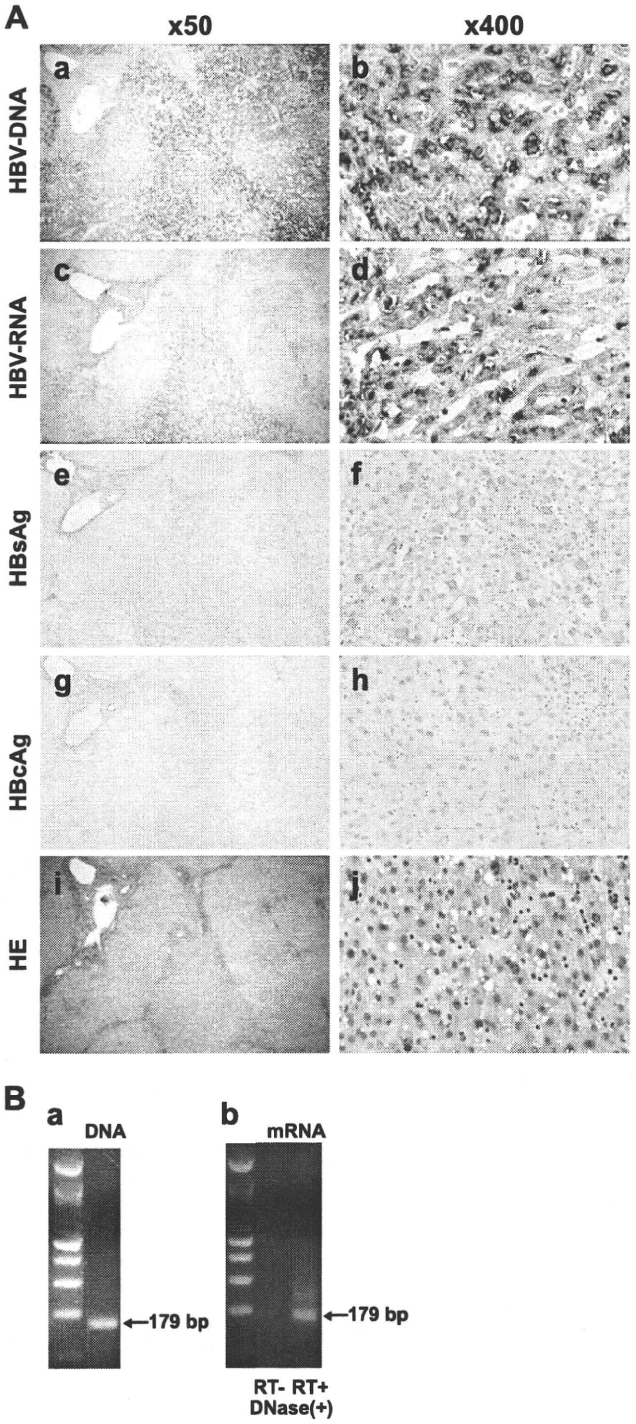

FIG. 3. (A) Panels a to h, HBV DNA, HBV RNA, HBsAg, and HBcAg detected in OCT-embedded frozen liver tissue from a patient with chronic hepatitis B by PCR-ISH (panels a and b), RT-PCR–ISH (panels c and d), and immunohistochemical staining (panels e to h). Panels i and j, HE staining of serial sections. The primers and probe targeted the S region to detect HBV DNA and HBV RNA. Antibodies to the envelope and core proteins were used to detect HBsAg and HbcAg, respectively. Magnifications, ×50 (panels a, c, e, g, and i) and ×400 (panels b, d, f, h, and j). The number of PCR cycles was 42. (B) Amplified DNA fragments in the PCR mixture of the section in panel A. Panel a, the DNA fragments amplified by 42 cycles of PCR were visualized by 3% agarose gel electrophoresis. Panel b, RT-PCR after DNase I treatment (3 U/μl) and negative controls (no RT).

tissue from the patient with HBV and HCV coinfection, there was an intense hybridization signal for HCV RNA on RT-PCR–ISH in almost all the hepatocytes (Fig. 5A, panel b). There was also a positive but weak RT-PCR–ISH signal for HCV RNA in the tumor hepatocytes (Fig. 5B, panel b). Few hepatocytes in the cancerous tissue were positive for HBV DNA by PCR-ISH (Fig. 5B, panel a), and no HBV DNA hybridization signal was detected in the noncancerous tissue (Fig. 5A, panel a).

DISCUSSION

The standard assay for detecting replication of HBV and HCV in tissue is ISH, but results are often inconsistent and sometimes difficult to reproduce. The specificity of ISH is high but its sensitivity low, and it is difficult to detect low copy numbers of the HBV or HCV genome in tissue. PCR technology has been adapted to *in situ* amplification of viral genomes or their replicative intermediates in liver tissue sections, but sensitivity and specificity remain major challenges to the application of this approach (13, 18, 23, 25, 26, 30, 31). Here, we describe the use of a novel, highly specific and sensitive PCR-ISH method to determine the distribution and localization of HBV DNA, HBV RNA, and HCV RNA in both normal and cancerous liver tissues.

PCR-ISH is the most sensitive technology currently available for the detection of viral genomes, but a major potential limitation of this approach is the low specificity. We were able to improve the specificity of PCR-ISH by careful optimization of certain steps. PCR was performed using sets of antisense and sense primers that were complementary to the sequences located in the S and X regions of HBV and the 5′-UTR upstream of the core region of HCV. We added PCR templates to the PCR mixture and then added the PCR mixture to the HBV- or HCV-negative tissue sections. The slides were placed in the GeneAmp *in situ* PCR system 1000 unit, and PCR-ISH was performed as described in Materials and Methods. Following these results, we selected the primer and probe set that did not stain the HBV- or HCV-negative tissue sections by PCR-ISH. Second, the type and concentration of protease and the treatment time were adjusted to optimize permeabilization of membranes and release of protein-nucleic acid cross-linking while avoiding overdigestion. Third, to improve the specificity for detecting viral genomes, we limited the number of PCR cycles and fixed the liver tissue sections in 4% paraformaldehyde immediately after PCR amplification. This step is essential to avoid diffusion of PCR products into neighboring cells, a phenomenon known as the diffusion artifact. Limiting the number of PCR cycles was also important for eliminating the background staining, as too many cycles resulted in high background staining and loss of tissue morphology. Fourth, we added a DIG-dUTP tail at the 3′ ends of the probes for PCR-ISH and RT-PCR–ISH. These 45-mer probes were optimized to improve their sensitivity without impairing the specificity.

HBV DNA was detected by PCR-ISH in a large number of hepatocytes in tissue sections from an HBV DNA-seropositive patient (Fig. 1A, panel a). HBV DNA was also observed by PCR-ISH in tumor hepatocytes in a section of cancerous tissue from the same patient (Fig. 1A, panel b). As shown in Fig. 2A,

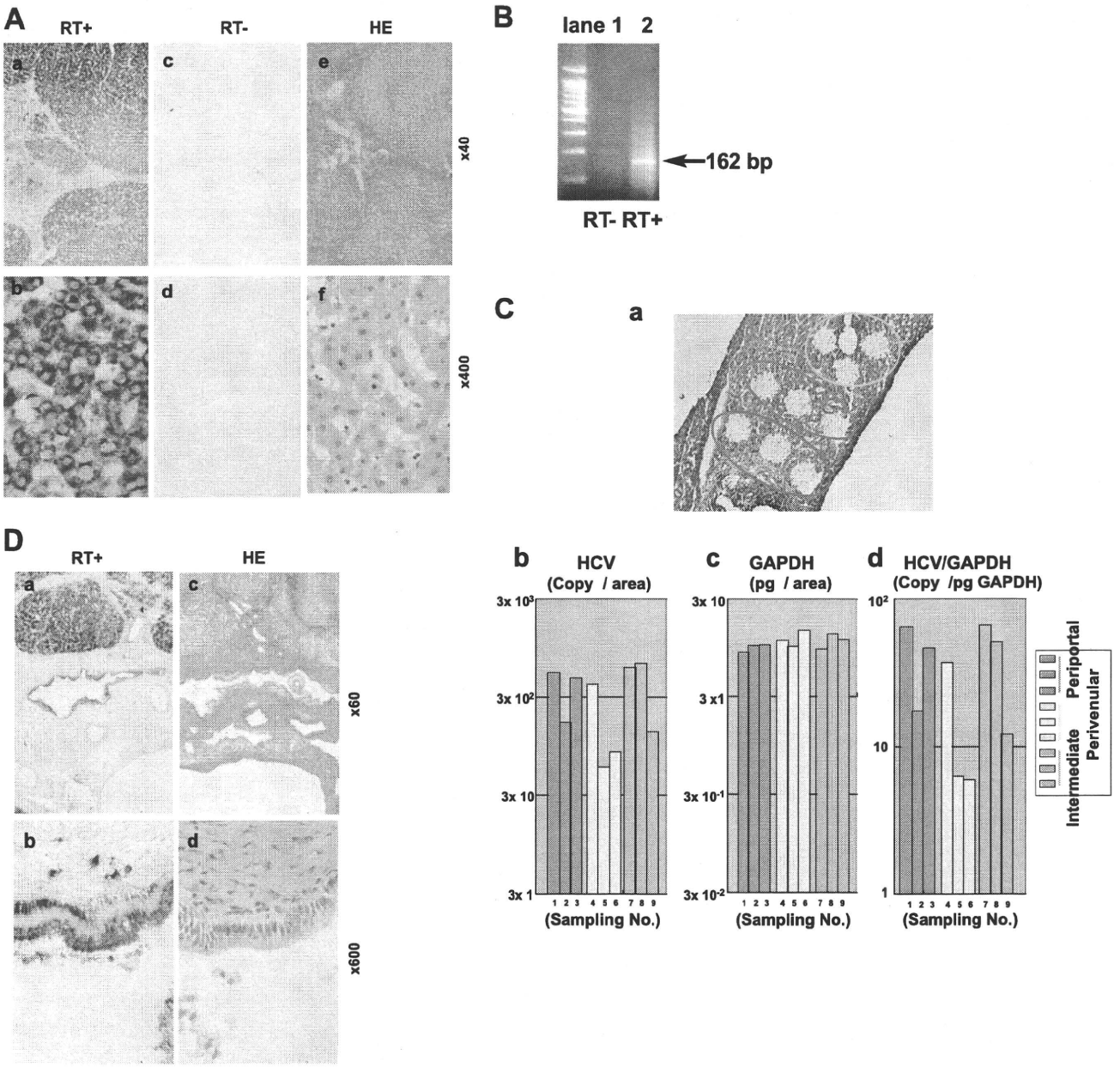

FIG. 4. (A) Panels a and b, HCV RNA detected in liver tissue samples from a patient with chronic hepatitis C by RT-PCR–ISH. Panels c and d, HCV RNA was not detected in a negative control (no RT). The number of PCR cycles was 45. Panels e and f, serial sections were stained with HE. Magnifications, ×40 (panels a, c, and e) and ×400 (panels b, d, and f). (B) DNA fragments in the PCR mixture of the section in panel A were amplified with the RT step and detected by 3% agarose gel electrophoresis. Amplification without the RT step resulted in no detection of DNA fragments. (C) Panel a, after LCM of nine areas, sections of liver tissue obtained from a patient with chronic hepatitis C were stained with HE. Panels b and c, HCV RNA and GAPDH mRNA in each of the areas were quantified by RTD-PCR, and the results are expressed as copy number per LCM area. Panel d, the copy number of HCV RNA was corrected by using the picogram weight of GAPDH. (D) Panels a and b, HCV RNA detected in the epithelium of the large bile duct by RT-PCR–ISH. The number of PCR cycles was 45. Panels c and d, serial sections were stained with HE. Magnifications, ×60 (a and c) and ×600 (b and d).

we obtained clear and reproducible patterns of distribution or localization of the viral genomes in the tissue sections. The visual patterns of HBV DNA distribution were similar, irrespective of the primer sets and probes (Fig. 2A, panels a to d). These data indicate that our technique is highly specific and reproducible for the detection of HBV DNA.

The staining pattern of HBV RNA was similar to that of HBV DNA (Fig. 3A, panels c and d). HBV DNA was also observed by PCR–ISH in tumor hepatocytes in a section of cancerous tissue from an HBV DNA-seropositive patient (Fig. 1A, panel b), but neither HBsAg nor HBcAg was detected in this section (data not shown). As shown in Fig. 3, the intensity of HBV DNA by PCR-ISH was almost the same as that of HBV RNA by RT-PCR–ISH but did not coincide with the